A Novel Demonstration of Squeezed Quantum Spatial Mode Reconstruction

A thesis submitted in partial fulfillment of the requirement
for the degree of Bachelor of Science with Honors in
Physics from the College of William and Mary in Virginia,

by

Kalea Huei-mei Wen

Advisor: Professor Eugeniy E. Mikhailov

Professor Saskia Mordijck

Professor Patel Mainak

Professor Gregory Bentsen

Williamsburg, Virginia
May 8, 2026

Contents

Acknowledgments

I would like to sincerely thank my advisor Professor Mikhailov for all the hours of mentoring and infinite patience he has given me as I learned the basics of this setup. Him and my co-advisor Professor Novikova have been invaluable to my undergraduate education and future career. I truly cannot express my gratitude in a way that captures how much I appreciate them. The entire W&M Quantum optics group, undergraduates and graduates, have always been helpful and inspiring peers as well. I am so grateful to be able to befriend, learn and grow along side them. I want to additionally extend my deepest admiration and appreciation to the all the incredible researchers that pioneered this project before me: Charris Gabaldon and Savannah Lea Cuozzo. Lastly I want to thank my mom and dad for calling me constantly while in the lab. What a privilege it is to a have doting wonderful parents!

List of Figures

List of Tables

Abstract

Quantum systems naturally contain tiny fluctuations, or "noise," that can limit the precision of sensitive measurements and sensing technologies. One way to reduce this noise is through a special quantum state of light called squeezed light, which redistributes fluctuations to improve measurement precision by reducing noise in either certain properties of light. My research explores how squeezed light can exist in multiple overlapping spatial patterns, a feature that may be useful for future quantum communication and networking technologies. In this work, I experimentally demonstrate a new method for detecting and reconstructing up to four overlapping spatial modes of squeezed light using programmable optics, phase sensitive detection, and statistical analysis techniques.

Chapter 1

Motivation

The goal of this research on a broad level is to make discoveries, protocols, and new technologies that advance the field of Quantum Metrology, which is the pursuit of quantum enabled high precision measurement tools. A measurement in an experimental, or real-world, setting can be simply described as the sum of the **desired signal**, and **noise** from any relevant region of the experimental device. The ratio of signal power to noise power, commonly called the "SNR," bounds the possible measurement precision of an apparatus and the observed value of the mean [1]. High precision measurement applications require maximizing the SNR. This can occur by either enhancing the response of the signal to a given change in the system, or reducing the noise of the measurement.

In applications where light is used as a measurement tool, the amplitude and phase of the electromagnetic wave is of interest. Noise can be defined as an uncertainty in the measurement of either of these quantities, revealed by disagreement in values between multiple measurement events. This noise could be identified by laser frequency and intensity instabilities, acoustic vibrations, temperature fluctuations, or some type of ambient mechanical oscillation. Techniques such as active feedback locking, and reference beams can greatly reduce or eliminate classical effects. However, scientists in the 20th century discovered that fundamental fluctuations exists even in the absence

of all classical disturbances. This is referred to as quantum noise and is considered an intrinsic property of light, described by the Heisenberg uncertainty principle. One could believe this standard quantum limit, or SQL, then bounds the maximization of the SNR in classical observations and noise reduction schemes. Luckily, this is not exactly the case.

My research involves the generation and study of Squeezed Light, a powerful quantum tool that allows for noise reduction schemes to surpass the SQL. Consider a state of light that is classically optimized to the SQL of noise in both the phase and amplitude quadrature. Squeezing the light redistributes the fundamental quantum noise, allowing for below-SQL noise levels in either the phase or amplitude quadrature of light at the expense of above-SQL noise levels in the conjugate quadrature [2]. However, more precise measurement capabilities are not the only result of optical squeezing. Non-classical states of light, specially a single squeezed beam, have unexplored spatial distributions and transverse-spatial-mode (TSM) structures [3]. Such quantum structures are overlapping and not detectable classically, but have potential usage in quantum information applications. In quantum networking for example, each unique quantum spatial mode could store information in their squeezing parameter. Unlike modern day quantum networking frameworks, our system could resolve as many quantum modes as desired within power-limits. This work contributes to the foundation of possibly the first high-dimensional quantum networking pursuits. Additionally, probing effects of squeezed light can illuminate new possibilities and research directions in quantum metrology and imaging. Therefore, I will demonstrate a method to detect and reconstruct individual spatial modes, or channels, of light from a squeezed source.

This thesis will introduce the mathematical framework of optical squeezing and the nature of over-lapping spatial modes within a beam of light in chapter 2. In chapter

3 and chapter 4, I will discuss experimental methods and the data collection involved to measure the squeezed light source. In Chapter 5, I will discuss the postprocessing decomposition methods needed to reconstruct individually squeezed quantum spatial modes from the data. In Chapter 6 I will present the results of our experiment and its implications. In chapter 7 I will conclude this thesis.

Chapter 2

Theory

2.1 Classical Representation of Light

Light can be described as an electromagnetic wave, with its energy propagating through electric and magnetic fields that are perpendicular to each other and the wave's direction. The electric field can be generally expressed as

$$\hat{E} = E_0 e^{i(\vec{k}\cdot\vec{r}-\omega t+\phi)}, \tag{2.1}$$

where E_0 is the amplitude of the electric field, e is Euler's number, $\vec{k}$ is the direction of propagation, $\vec{r}$ is a position in reference to an observer, w is the angular frequency of the wave's oscillations, t is time, and ϕ is the initial phase of light. The amplitude and phase of light are fundamental characteristics of light and are of interest in measurement applications. By Euler's formula, the electric field can be described in real and imaginary components. This can be visualized in figure 2.1, showing both the imaginary and real components of an instance of the electric field as a black cross. Physical measurement of the intensity of light correspond to the amplitude of its electric field, which is a projection of a measurement "point" onto the real axis. The phase of the electric field, defining the phase of the light, can be found through the projection of this measurement "point" onto the imaginary axis.

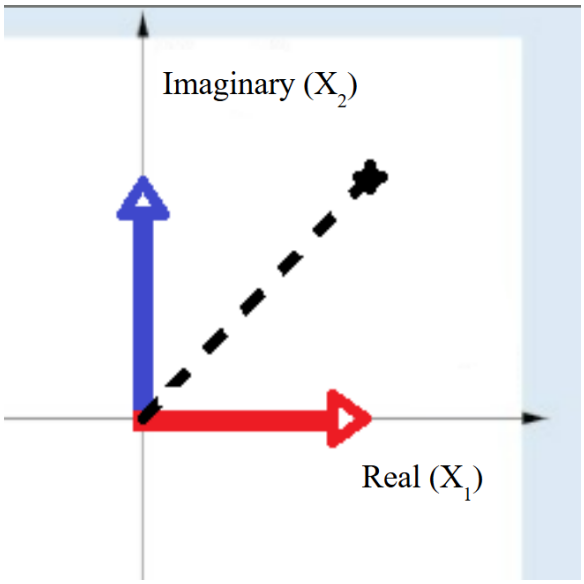

Figure 2.1: Real and imaginary components of an instance of an electric field. This is also known as phase space.

However this definition is not the full picture. Light is both a wave, as described in equation (2.1), and a collection of particles called photons.

2.2 Quantum Representation of Light

Squeezed light is a quantum phenomenon requiring a quantum definition of light. The properties of amplitude and phase still apply. The measured intensity of light is determined by the continuous flow of many photons carrying discrete amounts of energy, where more photons mean higher intensity. The quantized amount of energy of each photon relates to its frequency or color. Mathematically the precise number of photons and their quantized energy is represented by

$$\hat{N}|n\rangle = n|n\rangle, E_n = \hbar\omega(n + \frac{1}{2}), \tag{2.2}$$

where $|n\rangle$ is called a number state, n is the photon number and $\hat{N}$ is called the number operator, defined as $\hat{N} = \hat{a}^\dagger\hat{a}$. $(\hat{a}^\dagger)$ is known as the creation operator and $(\hat{a})$

is the annihilation operator. Creation and annihilation operators can be applied to a number state as

$$\hat{a}^\dagger|n\rangle = \sqrt{n+1}|n+1\rangle, \hat{a}|n\rangle = \sqrt{n}|n-1\rangle, \tag{2.3}$$

One can now derive the form of a quantized electric field propagating along the $\hat{z}$ direction as

$$\hat{E} = E_0(\hat{a}^\dagger e^{-i\omega t} + \hat{a}e^{i\omega t})e^{i(\vec{k}z-\omega t)}, \tag{2.4}$$

where E_0 is the electric field amplitude, ω is the angular frequency of the electric field, $\vec{k}$ is the wave vector, mentioned previously, and is defined as $\vec{k} = \frac{\omega}{c}$, and t is time.

2.3 Quadrature Space

The visual in figure 2.1 of the electric field of light exists in an abstract mathematical representation of all its relevant properties called phase space. Phase space is a useful representation as it depicts correlations between observables that cannot both be measured to exact precision at the same time. In figure 2.1, the observables are the measurable amplitude of light and the imaginary phase of such instances of measured light. These are called the real, X_1 or q, and imaginary, X_2 or p, axis respectively, or quadratures. In phase or quadrature space, they can be expressed as

$$\hat{q} = \frac{1}{\sqrt{(2)}}(\hat{a}^\dagger + \hat{a}) \tag{2.5}$$

$$\hat{p} = \frac{1}{i\sqrt{(2)}}(\hat{a}^\dagger - \hat{a}). \tag{2.6}$$

X_1 and X_2 are directly proportional to the canonical position $\hat{q}$ and momentum $\hat{p}$ operators from quantum mechanics. The Heisenberg Uncertainty Principle dictates that these quadratures satisfy a similar commutation relation of position and momentum:

$$[\hat{q}, \hat{p}] = i\hbar \tag{2.7}$$

In this thesis, X_1 and X_2 and $\hat{q}$ and $\hat{p}$ will be used interchangeably.

Quadrature space can provide insight to the noise present in different aspects of a system and how those aspects interact with each other. Take the case of many measurements of the electric field as shown in figure 2.2.

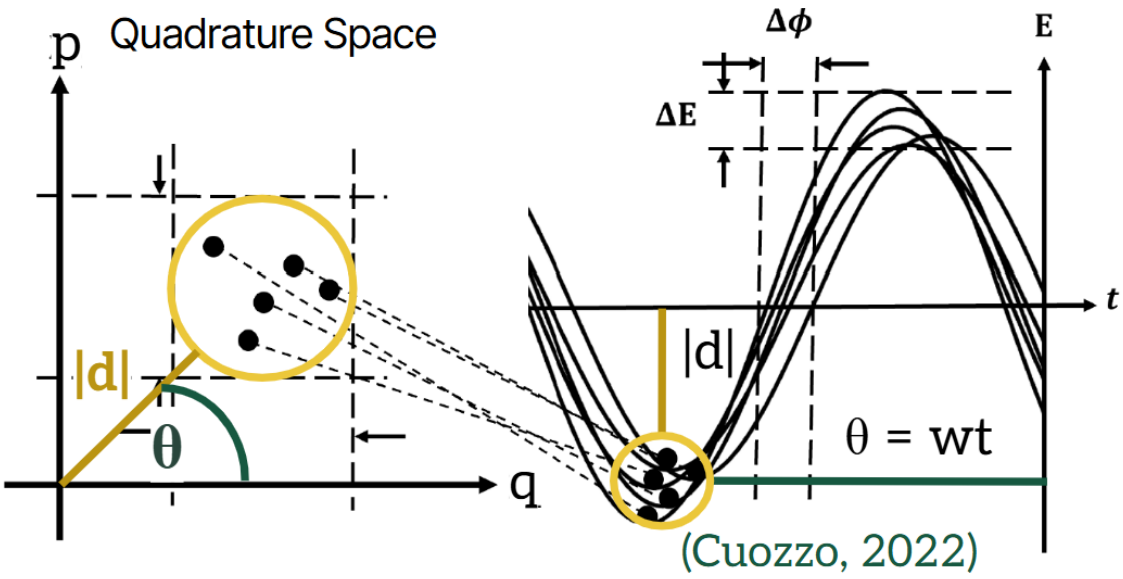

Figure 2.2: Phase space representation (left) and real space representation of an electric field (right). Figure from [4].

Compared to the single measurement in figure 2.1, we can see 5 distinct measurements of the electric field at slightly different times do not yield the same outcome and vary equally in phase (time) and amplitude as shown in quadrature space. The value $|d|$ and θ represent the mean amplitude and phase of the signal respectively. The yellow circle denotes the noise component of the measurement.

Notice that the length of each quadrature displaced from the origin makes up the mean or signal component of the phase (p quadrature) and amplitude (q quadrature) and is shown in green and yellow respectively. This is another way to describe the light that is equivalent to phase and amplitude. This is highlighted in figure 2.3.

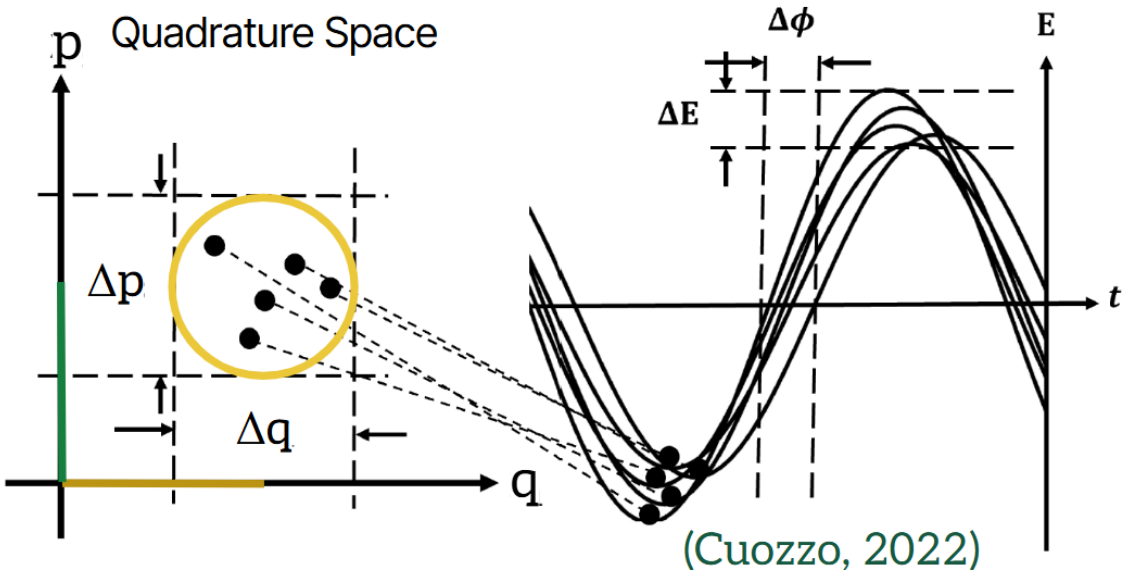

Figure 2.3: Phase space representation (left) and real space representation of an electric field (right). Figure from [4].

The product of each quadrature's statistical variances, or the lengths of the q and p portions of the noise ball, make up the effective area of the yellow circle in phase space. These quantities must obey

$$\langle(\Delta\hat{q})^2\rangle\langle(\Delta\hat{p})^2\rangle = 1. \tag{2.8}$$

This is a result of equation (2.7) and is fundamental to all measurements and normalized to a value of 1. The area of uncertainty in quadrature space is commonly referred to as a "noise ball."

If the noise ball has the absolute minimal quadrature variance product of 1 as expressed in equation (2.8), and the noise is evenly distributed in all quadratures,

then the light can be described as a coherent state. In experimental practice, this minimum uncertainty is often rescaled by a normalization of the quadratures such that the vacuum (or coherent state) variance corresponds to a value of 1, defining the shot noise level (or standard quantum limit). A coherent state occurs at any zero or non-zero amplitude of a light field. Often the noise ball can have a larger quadrature variance product than a coherent state, raising the uncertainty of measurement. This is called a thermal mode and its noise is outside of the quantum standard limit and could be from classical sources of fluctuations. Coherent states and thermal states are shown in figure 2.4.

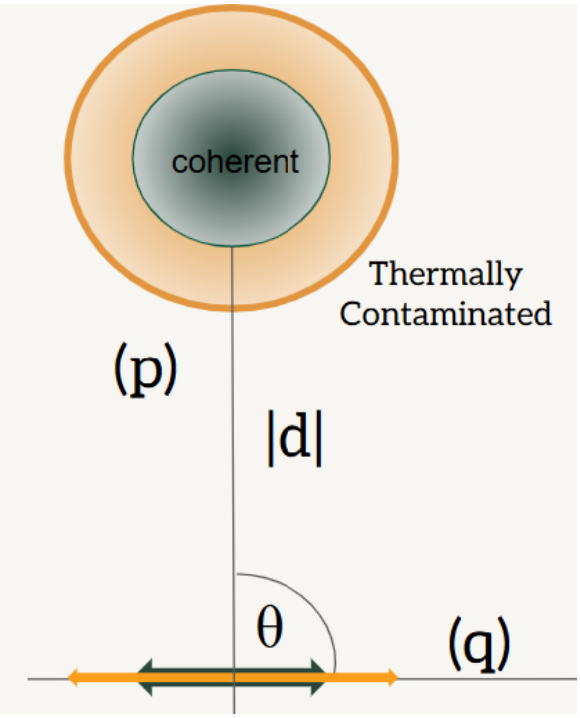

Figure 2.4: Coherent mode in green, and a thermal mode of light in orange.

2.4 Squeezed Light

While the area of a noise ball is bound by the Heisenberg Uncertainty Principle as given in equation (2.8), this does not dictate the distribution or shape of our noise

ball. Experimentally, it is possible to "squeeze" or redistribute the noise in quadrature space such that the "noise ball" is not equally distributed in each quadrature. If the size of the noise distribution is below the SQL in the amplitude or phase direction, then the state is optically "squeezed." As a result, one portion of the noise ball will visually appear "shorter" than the coherent state and the other portion "longer". This is shown in the left of figure 2.5, where the green noise ball is a coherent state, and the yellow noise ellipse is a squeezed state. On the left, a real space plot of the electric field of such squeezed modes in phase space are shown as well. Amplitude squeezing is visible in real space by a decrease in the noise on the ε axis. However, this does not reveal the noise information of the phase component. Phase space plots fully capture all quadratures of light and are more commonly used as a result.

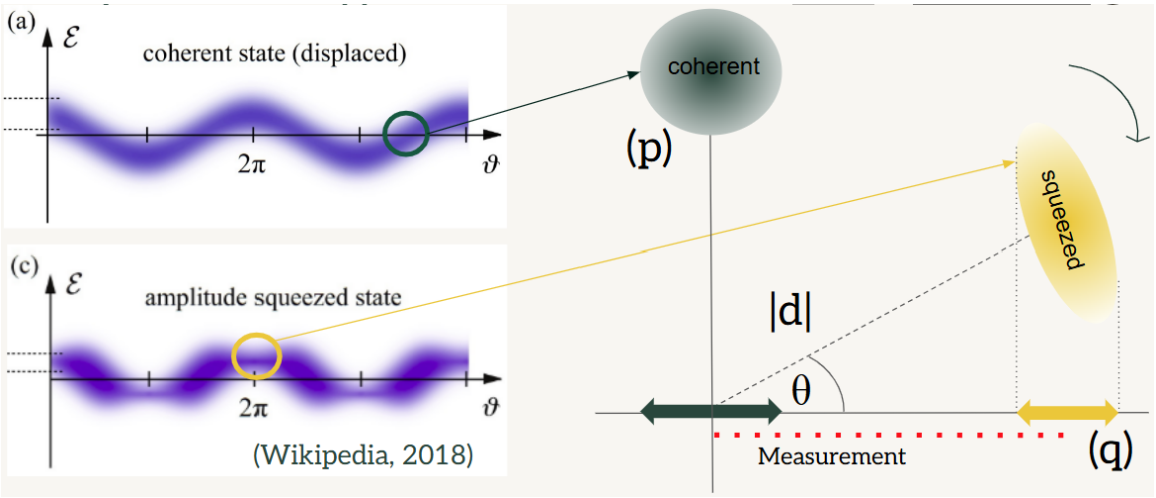

Figure 2.5: Coherent (green) verse squeezed state (yellow) in quadrature space and their possibly real space measurements in purple. Figure from [5].

Its important to understand that the shorter (squeezed) axis of the blue squeezed state in the figures possesses less noise than the standard quantum limit of precision, while the larger (anti-squeezed) axis posses more. In other words, squeezed states supress the fluctuations in one quadrature such that $\langle (q)^2 \rangle \neq \langle (p)^2 \rangle$ [2]. Squeezed light states can be engineered such that the one measurement quadrature of interest

always has less noise than the standard quantum limit, making them useful in sensing and metrology applications.

Squeezed states can also occur in vacuum and are shown below in the right of figure 2.5. There is no classical amplitude shown in the phase space diagram, resulting in the mode being "centered" at the origin. This research creates vacuum squeezed states.

We can mathematically describe single-mode squeezing on some mode n as

$$\boldsymbol{S}(\zeta_n) = e^{\frac{1}{2}(\zeta_n^* \hat{a}^2 - \zeta_n \hat{a}^{\dagger 2})}, \zeta = r_n e^{i\theta_n} \tag{2.9}$$

where the creation operator, $(\hat{a}^\dagger)$ and annihilation operator $(\hat{a})$ are quadratic terms. This is because squeezing is a non-linear process involving the creation or annihilation of photons in pairs. r_n is the squeezing parameter which quantifies the degree of squeezing and θ_n is the squeezing angle.

2.4.1 Thermal State

True squeezing is assume to be applied to a coherent state of light, as pictures in figure 2.4. Squeezing operators can be applied to states that are noisier than shot noise as well. These states are called thermal modes and are a statistical mixture of number states [2]. A thermal state is different from a coherent state because it exhibits increased quadrature variance without displacement in phase space from the origin as shown in figure 2.4. A coherent state would have the same noise properties as a vacuum state (shot noise limited) and be displaced some $|d|$. When a thermal mode is squeezed, the noise still unevenly distributes and could result in optical squeezing, or noise below the shot-noise limit in one quadrature. However, the resulting squeezing will always be less than that of a coherent state when squeezed.

2.5 Multi-mode Squeezing

Optical squeezing occurs by many methods, often depending on the application. In this research, squeezed states of light are generated in a process described as Polarization Self Rotation (PSR) through a hot vapor cell. No other experimental instruments, like an optical cavity, are used to constrain or filter the generation of squeezed signals. For this reason, our experiment creates an unknown amount of multi-mode squeezing at a single frequency. Within a single laser beam, the squeezed output can be described as a superposition of many uniquely squeezed individual modes, or each distinct n found from equation (2.9). Therefore measuring N constituent squeezed modes can reveal the quantum spatial mode structure present in the squeezed source.

A spatial mode is a distinct transverse shape or intensity pattern of a light beam that define how the beam propagates and carry information. Without special equipment, it is not possible to detect quantum spatial modes within a beam as there structure is not visible unless exposed to a non-linear process. When the squeezer is applied, every unique spatial mode within the light will react differently and yield a unique r_n and θ_n. This distinct spatial modes mapping to unique squeezed noise distributions in quadrature space is symbolically shown in figure 2.6. The squeezed modes are overlapped and scrambled together, as expected within a single beam. Each blue arrow in the figure connects a symbolically distinct shape, like the cloud or heart, to a unique phase space distribution. The spatial modes in our experiment do not look as pictured in figure 2.6 however. The presentation of a heart or cloud just symbolically visualizes orthogonal elliptical spatial modes that are otherwise hard to imagine.

Multi-mode squeezing is more complex than single mode but offers more opportunities to take advantage of its richer structure for quantum information applications,

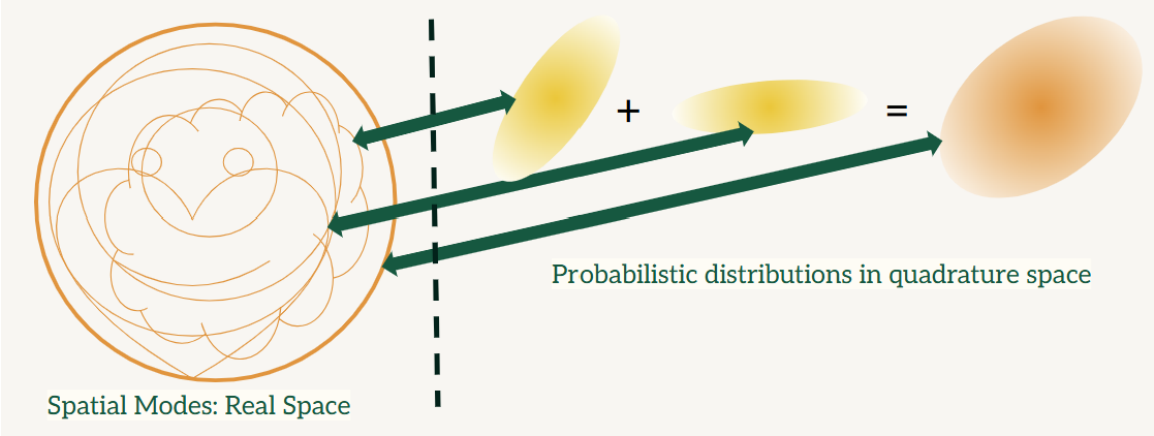

Figure 2.6: Symbolic visualization of unique overlapping spatial modes (left). Superposition of multiple orthogonal squeezed modes in phase space (right)

as will be discussed later.

2.5.1 Vacuum Squeezed Modes

The method of squeezing used in this experimentation creates multiple modes as discussed, but also such modes are at what is known as "vacuum." Vacuum means the absence of light/signal, or the lack of any photons. A measurement is made of both a signal and noise component however, so the noise distribution or "noise ball" will still exist even for a vacuum state. Such states visually appear to be located at the origin of the quadrature space as they do not possess a classical amplitude. Despite intuition, the noise ball at vacuum is not necessarily smaller than the noise ball at a non-zero amplitude. A vacuum mode will have minimal quadrature noise. Vacuum states are ideal for squeezing in this experiment as they are simpler than squeezed sates with mean amplitude as well. The coherent input to our squeezer is shown in green at vacuum, and the multi-mode squeezed output is shown in yellow in figure 2.7.

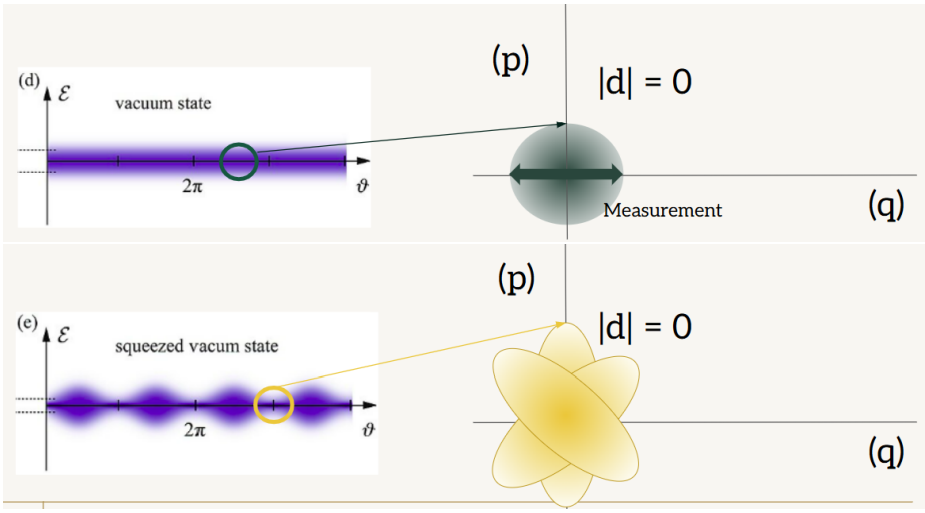

Figure 2.7: The input (green) and output (yellow) of light states through our experimental squeezer.

2.6 Gaussian States

We can mathematically represent a quantum state in phase space using a "quasi-probability" distribution called the Wigner Function. The Wigner function for gaussian modes is given below as

$$W(\mathbf{X}) = \frac{1}{(2\pi)^N \sqrt{\det \Sigma}} \exp\left[-\frac{1}{2}(\mathbf{X}-\bar{\mathbf{X}})^T \Sigma^{-1} (\mathbf{X}-\bar{\mathbf{X}})\right] \tag{2.10}$$

where N is the number of quantum modes in the system, Σ is the covariance matrix of the quadratures of all modes, and X is the phase-space vector for N modes given below.

$$\mathbf{X} = \begin{pmatrix} q_1 \\ p_1 \\ q_2 \\ p_2 \\ \vdots \\ q_N \\ p_N \end{pmatrix} \in R^{2N} \tag{2.11}$$

The light fields used in this research are Gaussian states, meaning their respective Wigner functions have a Gaussian distribution in phase space. Gaussian states produce elliptical squeezed states in phase space, which remain Gaussian in this transformation. It is possible to produce non-elliptical squeezed states or negative Wigner function values, hence its description as a "quasi-probability" distribution, but this will not occur in the case of Gaussian states.

Not every covariance matrix Σ is physically allowed. The quadrature variances must satisfy the uncertainty principle, which in normalized units can be expressed as

$$\langle(\Delta\hat{X}_1)^2\rangle \langle(\Delta\hat{X}_2)^2\rangle \geq 1, \tag{2.12}$$

as mentioned earlier. This implies that the covariance matrix Σ must correspond to variances and correlations that do not violate this bound, ensuring the state is physically realizable.

Gaussian states are characterized by the first two moments of their Wigner Functions, the first moment being the mean of the quadrature operators given in equations (2.5) and (2.6)

$$\bar{\mathbf{X}} = \langle\hat{\mathbf{X}}\rangle = \begin{pmatrix} \langle\hat{q}_1\rangle \\ \langle\hat{p}_1\rangle \\ \vdots \\ \langle\hat{q}_N\rangle \\ \langle\hat{p}_N\rangle \end{pmatrix} \tag{2.13}$$

. The brackets $\langle\rangle$ denote the quantum expectation value of an operator. If the quantum state is at vacuum, or centered at the phase space origin, all first moments will be zero. The second moment is the covariance matrix given as

$$\Sigma_{ij} = \frac{1}{2}\left\langle \hat{X}_i\hat{X}_j + \hat{X}_j\hat{X}_i \right\rangle - \langle\hat{X}_i\rangle\langle\hat{X}_j\rangle = \frac{1}{2}\left\langle \hat{X}_i\hat{X}_j + \hat{X}_j\hat{X}_i \right\rangle = c(X_i, X_j), \tag{2.14}$$

where $\hat{\mathbf{X}}$ is

$$\hat{\mathbf{X}} = (\hat{q}_1, \hat{p}_1, \ldots, \hat{q}_N, \hat{p}_N)^T \tag{2.15}$$

for N modes. The covariance refers to the linear relationship between two variables and how each quantity will change with respect to the other. The simplest instances of covariance are the diagonal elements of the covariance matrix for some diagonal element "i," given as

$$c(X_i, X_i) = v(X_i), \tag{2.16}$$

where v and c are the variance and covariance calculations respectively. For a single mode, each covariance matrix element can be written as individual covariances of each mode. This is shown below:

$$\mathbf{\Sigma_{n=1}} = \begin{pmatrix} \langle \hat{X}_1^2 \rangle = v(q) & \frac{1}{2}\langle \hat{X}_1\hat{X}_2 + \hat{X}_2\hat{X}_1 \rangle = c(q,p) \\ \frac{1}{2}\langle \hat{X}_1\hat{X}_2 + \hat{X}_2\hat{X}_1 \rangle = c(p,q) & \langle \hat{X}_2^2 \rangle = v(p) \end{pmatrix}, \tag{2.17}$$

where $\hat{X}_1 = \hat{q}$ and $\hat{X}_2 = \hat{p}$. The diagonal elements are the variances of the quadratures, while the off-diagonal elements represent their covariance. Using this form and expanding to many modes, the covariance matrix for n-modes looks like

$$\Sigma = \begin{pmatrix} v(q_1) & c(q_1,p_1) & c(q_1,q_2) & c(q_1,p_2) & \ldots & c(q_1,q_n) & c(q_1,p_n) \\ c(p_1,q_1) & v(p_1) & c(p_1,q_2) & c(p_1,p_2) & \ldots & c(p_1,q_n) & c(p_1,p_n) \\ c(q_2,q_1) & c(q_2,p_1) & v(q_2) & c(q_2,p_2) & \ldots & c(q_2,q_n) & c(q_2,p_n) \\ c(p_2,q_1) & c(p_2,p_1) & c(p_2,q_2) & v(p_2) & \ldots & c(p_2,q_n) & c(p_2,p_n) \\ \vdots & \vdots & \vdots & \vdots & \ddots & \vdots & \vdots \\ c(q_n,q_1) & c(q_n,p_1) & c(q_n,q_2) & c(q_n,p_2) & \ldots & v(q_n) & c(q_n,p_n) \\ c(p_n,q_1) & c(p_n,p_1) & c(p_n,q_2) & c(p_n,p_2) & \ldots & c(p_n,q_n) & v(p_n) \end{pmatrix} \tag{2.18}$$

2.7 Reconstruction of a multi-mode source

This research creates many squeezed Gaussian vacuum quantum states of light. Using a multimode squeezer allows for more channels, or spatial modes, for quantum information applications to be available for usage. To isolate or fully classify these modes,

we must measure their covariance matrices, or the 2nd moment of their Wigner functions or Σ as defined in equation (2.18). This contains all the essential statistical characteristics of the system, enabling us to identify correlations between the variances in each quadrature measurement. From this the squeezing parameters can be calculated for each mode.

The workflow of this experimental demonstration of squeezed quantum spatial mode reconstruction is shown in figure 2.8. The red line shows the forward propa-

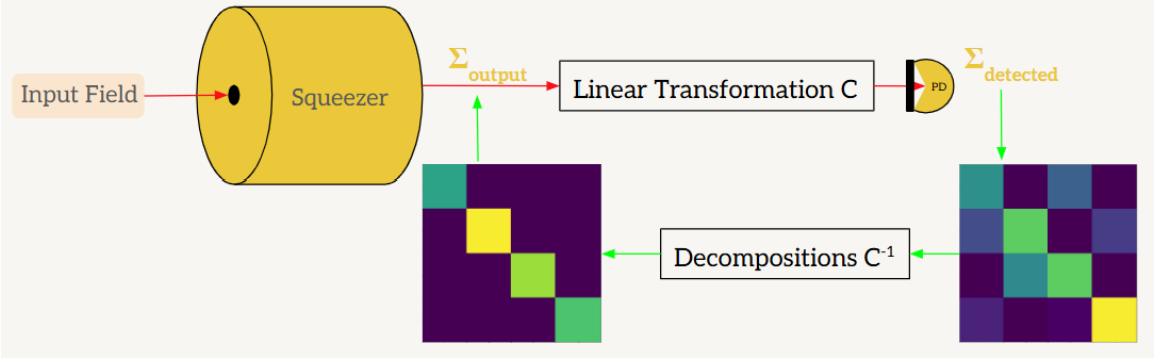

Figure 2.8: Reconstruction Workflow
In the forward propagation, Σ_o can be thought of as in a diagonalized basis after the squeezer. At the detector, Σ_O has undergone linear transformations from optical elements and is scrambled in the pixel basis. In the backward propagation, Σ is decomposed back into its mode basis. This figure was from [2].

gation of states and the green shows a backwards reconstruction. First, a hot vapor squeezer is used to generate multi-mode squeezed states at a single frequency. Such an ensemble can be described as a superposition of individually Gaussian squeezed states as shown in figure 2.6 and described fully by equation (2.18) or Σ_o. Multiple optical elements are required to detect this output, including beam splitters, waveplates and lenses that preserve all linear transformations as modes propagate. It is well-known that Gaussian states undergoing linear transformations will remain Gaussian [6]. Therefore, we can conclude that, in theory, information about the quantum spatial mode structure from our squeezed source is preserved at the detection output

Σ_d. Chapter 3 will explain the experimental measurement process in more detail.

However, Σ_d at the point of experimental measurement contains all linear transformations the system has undergone, effectively mixing the spatial mode structure. This is shown in figure 2.8, where the diagonalized covariance matrix, Σ_o, defines the modes of interest we ultimately want to reconstruct. To do this we first need to understand the forward propagation.

2.7.1 Forward Propagation

We can use the mode creation and annihilation operators, $\vec{A}_n = (a_1^\dagger, a_1, a_2^\dagger, a_2, \ldots, a_n^\dagger, a_n)$ to describe the mode diagonalized covariance matrix Σ_o right after the squeezer. We can say that Σ_o is in the modal basis. The optical measurement elements act on the mode operators $\vec{A}_n$ as a unitary transformation U, that we can define for the case of $n = 1$ as

$$\vec{A}_{d1}^{\,T} = u\vec{A}_{o1}^{\,T}, \tag{2.19}$$

where u is the individual transformation each $\hat{a_n}$ modes underwent from the squeezer (Σ_o) to the detector output (Σ_d). This can be extended to all $\hat{a_n^\dagger}$ in matrix U, where u and $u^\dagger$ make up its diagonal.

While U describes what physically occurs, measurements are performed in the quadrature basis as previously discussed. To describe Σ_d, we can use the quadrature operators, $\vec{X}_n = (q_1, p_1, q_2, p_2, \ldots, q_n, p_n)$. We can say that Σ_d is the projection of Σ_o in the pixel basis additionally.

The quadrature operators $\vec{X}_n$ are related to the mode creation and annihilation operators $\vec{A}_n$ through a fixed linear transformation. Recall from equations (2.5) and (2.6) that $\vec{X}_n$ is a linear combination of $\vec{A}_n$ for each element. To be precise,

we can define a matrix Q_n such that for $n = 1$

$$\vec{X_{O_1}} = \begin{pmatrix} \hat{q}_1 \\ \hat{p}_1 \end{pmatrix} = Q_1 \vec{A_{O_1}} = Q_1 \begin{pmatrix} \hat{a}^\dagger \\ \hat{a} \end{pmatrix} = \begin{pmatrix} 1 & 1 \\ i & -i \end{pmatrix} \begin{pmatrix} \hat{a}^\dagger \\ \hat{a} \end{pmatrix} \tag{2.20}$$

.

We can use this information to obtain the transformation done to the quadrature operators during the forward mode propagation, like in equation (2.19) for the modal operators. For the case of many modes n, we can see that

$$Q_n^{-1} \vec{X}_d = U Q^{-1} \vec{X}_o, \tag{2.21}$$

and we can write

$$\vec{X}_d = Q U Q^{-1} \vec{X}_o = C \vec{X}_o, \tag{2.22}$$

where we define $C = QUQ^{-1}$. This can be understood as the rotation of the modal basis (physical description) but expressed in the quadrature basis (measurement description). This is required as we cannot directly measure Σ_o, but only Σ_d. C is what as known as Symplectic, meaning that the area of the phase space distribution of the modes are preserved in transformation. This is required to maintain uncertainty principles of the noise.

Finally, as discussed in [2], the covariance matrix at the detector can be given as

$$\Sigma_d = C \, \Sigma_o \, C^T. \tag{2.23}$$

C is also an orthogonal matrix that satisfies the condition $C^{-1} = C^T$. Therefore we can write that

$$\Sigma_o = C^T \, \Sigma_d \, C^{\cdot} \tag{2.24}$$

Its important to note that this result is only possible with Gaussian states since the Wigner function behaves like a classical probability distribution [2].

Now we will proceed to discuss the experimental methods that produce such a transformation U on the spatial modes at the squeezer output in the next chapter. Once measured, a series of decompositions are applied to reverse the propagation of states through the optical elements, or all u_n, and identify the spatial modes through equation (2.24). Chapter 5 will explain this backward reconstruction or decomposition process in more detail.

Chapter 3

Experimental Setup

This section will describe the optical elements required to detect the squeezed output from figure 2.8. Specifically, the experimental apparatus will effectively apply the linear transformation, C, to the mode out of the squeezer as shown in figure 3.1.

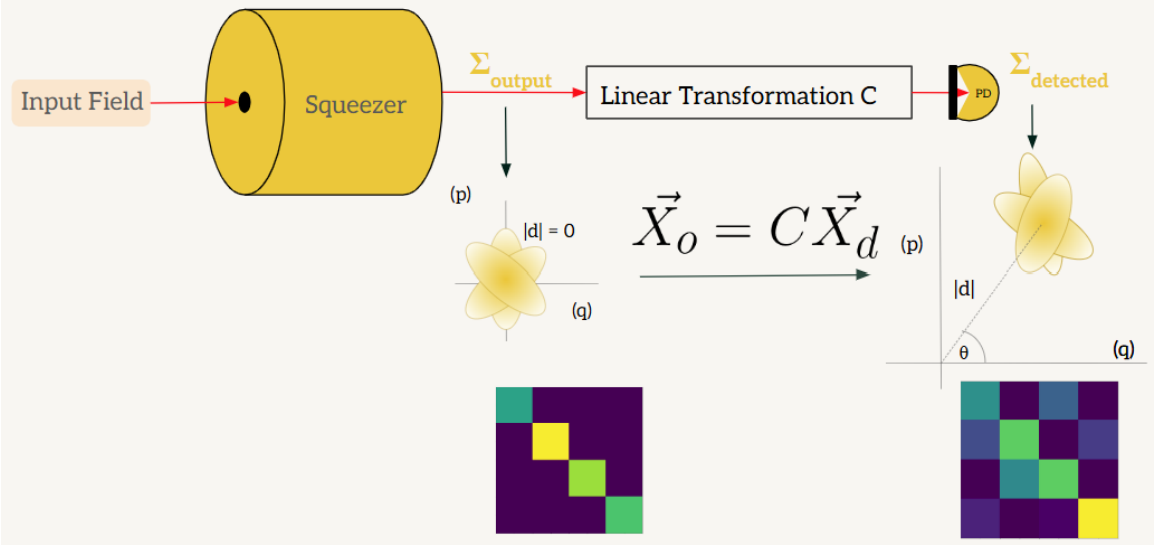

Figure 3.1: The experimental apparatus serves as a linear transformation to measure the multi-mode squeezed ensemble. The vacuum signal must be amplified and interrogated to do this, resulting in the propagation of the modes as shown in the covariance color maps.

The experimental setup is physically shown in figure 3.2. The path of the laser is shown in red.

A cartoon version of this optical path is shown in multiple parts on figure 3.3. The

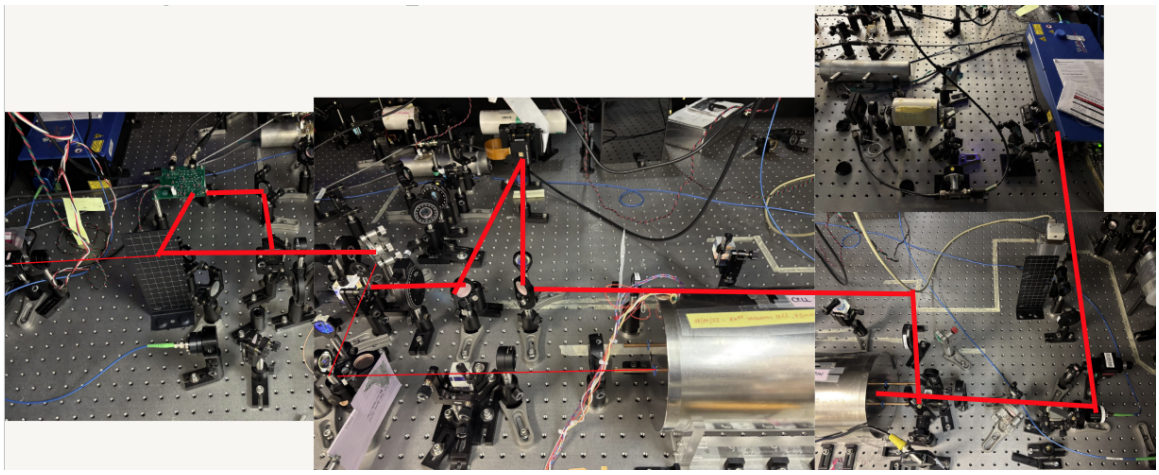

Figure 3.2: Real life setup.

squeezed signal is very weak and requires amplification to be measured. This setup interferes the squeezed signal with a stronger beam, or local oscillator (LO), with adjustable phase. The interference pattern generated between the beams for different LO phase masks reveal different aspects of the covariance matrix in equation (2.18). We will review every step of this process in this section.

3.1 Squeezing Generation

The method of Polarization Self-Rotation (PSR) is used to generate squeezing shown in part (a) of figure 3. This generation relies on the passage of a laser through an atomic vapor to induce polarization rotation. We use atomic Rubidium (^{87}Rb) due to simplicity, as it only has one valence electron and is easily accessible with near infrared lasers. The transition of interest is the D1 transition line (795nm) between $5^2S_{1/2}$ ground state and the $5^2P_{1/2}$ excited state shown in Figure 3.4.

When light passes through an atomic medium, it will experience an AC Stark shift due to the alternating electric field of the laser. If this light is elliptical polarized, the medium then becomes circularly birefringent. This occurs because elliptical light could be thought of as the addition of two unevenly circular polarized components:

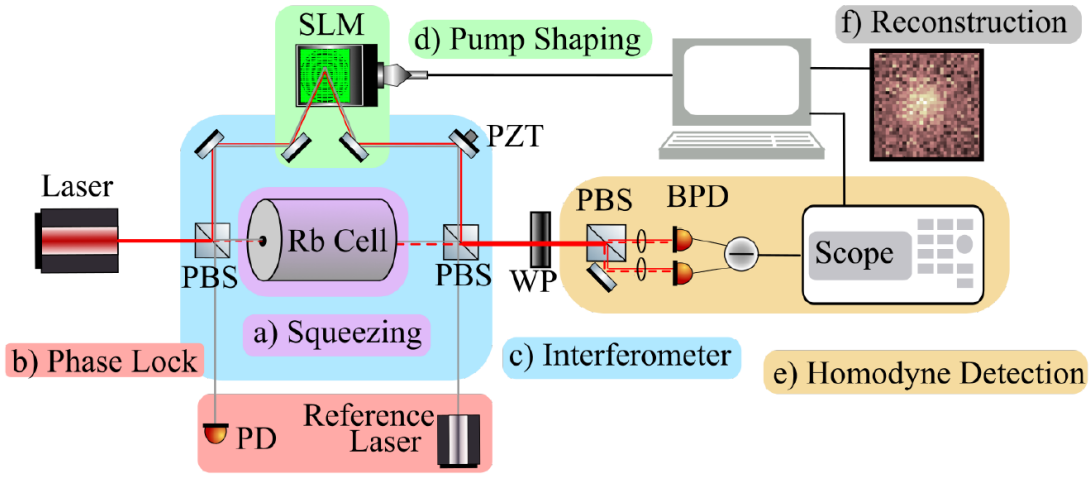

Figure 3.3: Experimental Setup
a) is the squeezing mechanism, b) acts as a phase reference for the local oscillator, c) is the interferometer of the probe/pump signal and the local oscillator, d) the is spatial light modulator used to shape the local oscillator beam, e) is the detection method used to see interference, and f) is the computational reconstruction post-processing phase of this research. This figure was made by Charris Gabaldon [2].

a right-handed and left-handed circularly polarized light. This results in the uneven shifting of degenerate ground states under the AC stark effect as shown by $|1\rangle$ and $|2\rangle$ in Figure 3.4. Each of these components will experience a different index of refraction while passing through atomic vapor. Therefore, rotation of the elliptically polarized light occurs as shown in figure 3.5. PSR in turn causes non-linear electric susceptibility from the atomic medium when interacting with the laser beam [2]. Squeezing can be generated experimentally in such non-linear interactions which results in the uneven distribution of quantum noise. PSR is not directly responsible for squeezing behavior, but both originate from the same nonlinear interaction [7].

In this experiment, we generate vacuum squeezing by passing linearly polarized light instead of elliptical into the hot vapor cell. This is called a pump field, and it serves as a source of correlated photon pairs for squeezing [8]. Macroscopically, no self-rotation occurs since the right and left hand components are even. However, the

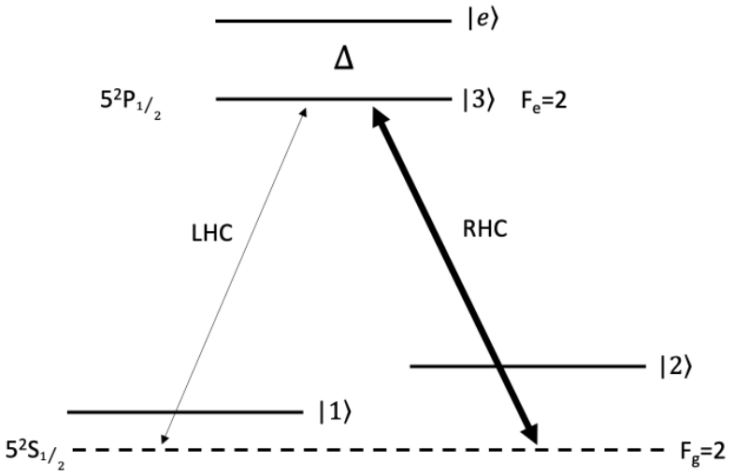

Figure 3.4: Rubidium lambda system
This figure is from [2].

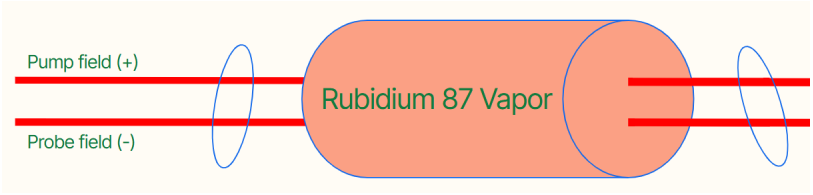

Figure 3.5: Polarizaiton Self-Rotation

same mechanism still couples the quantum noise from these two circular components and mediates the conversion of the pump photons into a squeezed pair of orthogonal polarization [7]. This produces a classical linearly polarized pump field and a squeezed vacuum field in the orthogonal polarization. The output is what is shown in figure 2.5.

Unfortunately in practice, there is polarization leakage from the pump field into the squeezed output. This results in vacuum and thermal states in the squeezed signal. The thermal modes degrade the squeezing as discussed in section 2.4.1. This fact will become important during post-processing of the data in chatper 5.

3.1.1 Optimal Squeezing

Obtaining the most amount of squeezing from our PSR method allows for possibly better contrast or resolution of the quantum spatial modes of interest. Experimentally, the laser de-tuning, laser power, and atomic density of Rubidium can be optimized for squeezing. Factors that impact the atomic density include the cell temperature and the point at which the laser focuses in the vapor cell.

We can currently achieve about 2.2 ± 0.24 db of squeezing, with a laser power at about 21mW in the signal arm upon entry into the cell, and a cell temperature at about 68 degrees C. The laser power was optimized at different cell locations relative to the focal point of the beam in figure 3.1.1. Additionally, the temperature of the cell was optimized in combination with the laser power and the best found cell "positions".

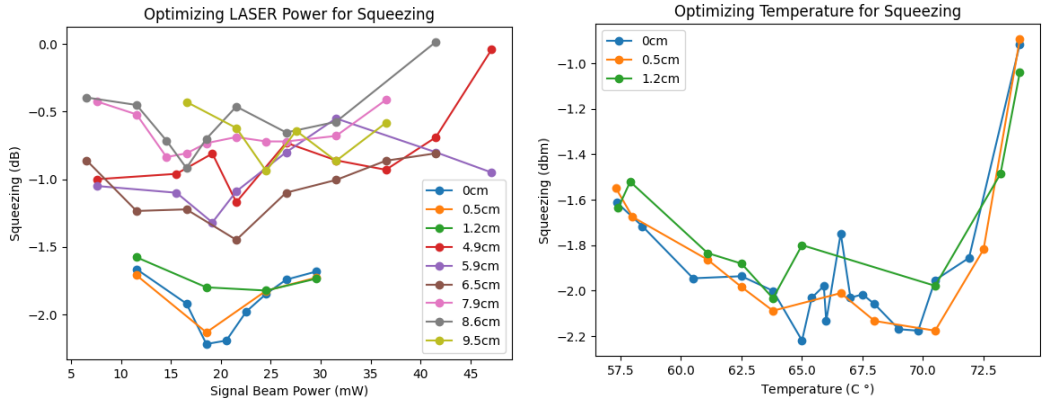

Figure 3.6: Squeezing optimization
The power was tracked through the response on 1 photo-diode through a ND filter. Each color corresponds to the distance of the center of the glass vapor cell of Rubidium to the approximate focal point of the laser.

The laser is blue de-tuned of the $F = 2 \rightarrow F' = 2$ by a few tens of MHz, from the transition of the $D1$ line of Rubidium shown in figure 3.7 for optimal squeezing.

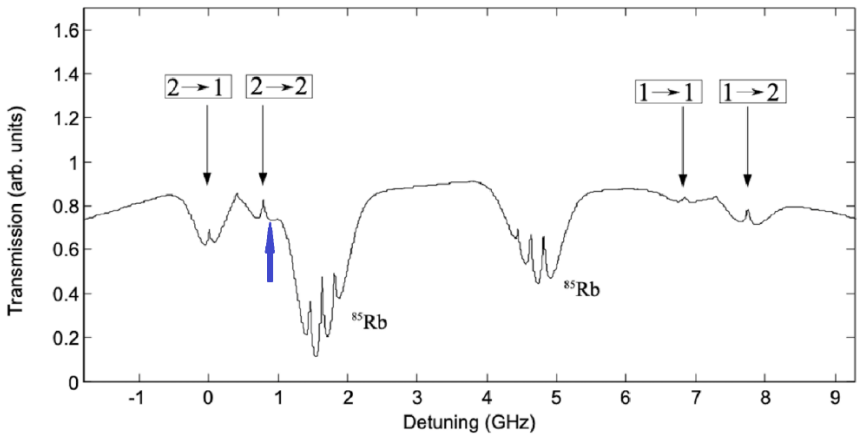

Figure 3.7: Resonances of Rubidium
Optimized squeezing occurs at the blue arrow. This figure is inspired from [2].

3.2 Interferometer

Measuring the squeezed vacuum state directly would be very difficult, as vacuum fluctuations are too weak to detect normally and will be hidden by the dark noise of the photodiode. Therefore we need to employ an amplification method that allows us to detect the output squeezing. Before the squeezer, the beam is split into the squeezed signal and LO paths, creating an interferometer shown in part (c) of figure 3.3. A piezoelectric transducer (PZT) is placed on one of the paths, creating a controlled interference pattern. Once recombined, the interference fringes reveal the rotation of the noise ellipse by θ about the phase space origin as shown in the left of figure 3.8. The PZT is set to sweep the full 2π period multiple times so that all possible dimensions of the noise ellipse are projected onto the real measurement axis. This interferometer enables measurement of both the maximum anti-squeezing (largest uncertainty) and squeezing (smallest uncertainty).

The signal and LO's mean field, or amplitude, can be described as α_{sig} and α_{LO} respectively. We can track the fluctuations of the fields with quadratures X_1 and X_2 such that the total field behavior can be described as

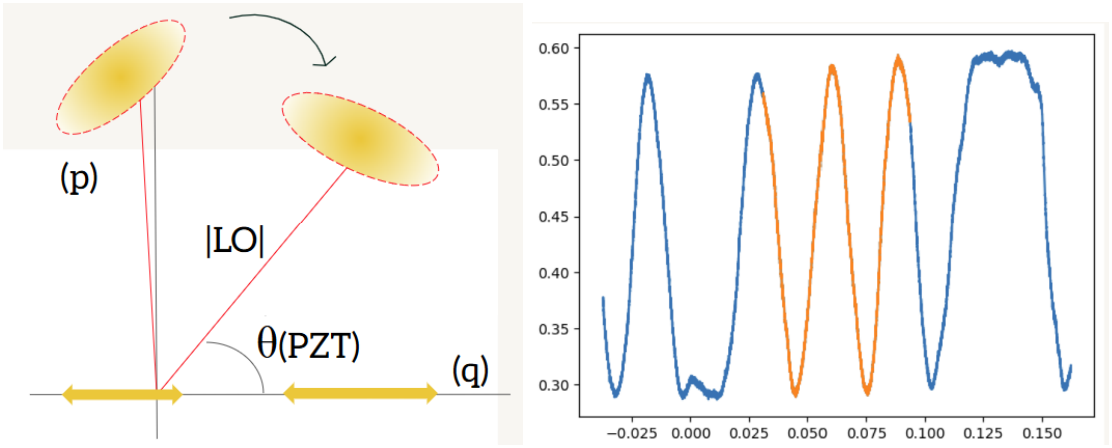

Figure 3.8: Left image: Solid red line represents the LO (or mean component) while the dashed red line represents the vacuum squeezed signal (or the noise component). The PZT will cause the rotation of the entire noise ball about the origin of phase space. Right image: The scope output of the PZT sweeping the amplitude of the measured output.

$$\hat{\alpha}_{sig}(t) = \alpha_{sig} + \hat{X}_{1sig} + i\hat{X}_{2sig}, \tag{3.1}$$

$$\hat{\alpha}_{LO}(t) = [\alpha_{LO} + \hat{X}_{1LO} + i\hat{X}_{2LO}]e^{i\phi_{lo}}, \tag{3.2}$$

where $e^{i\phi_{lo}}$ indicates the phase difference between the LO and signal beam [2]. Experimentally we are sweeping through this phase by changing the path length of the signal arm in the interferometer using the PZT. An example of the projection of a rotating noise ellipse during the PZT sweep is shown in figure 4.2.

3.3 Homodyning Detection Scheme

At the point of part (e) in figure 3.3, the squeezed signal and LO are mixed back together, but squeezing information is contained in the phase of the output. We employ homodyne detection, a phase sensitive measurement technique in quantum optics, to differentiate between the quadrature noises from this output [9]. Notably

this involves the subtraction of two detectors to cancel the intensity noise and just leave information about the squeezing as noise quadrature projections. This detection scheme is pictured in figure 3.9.

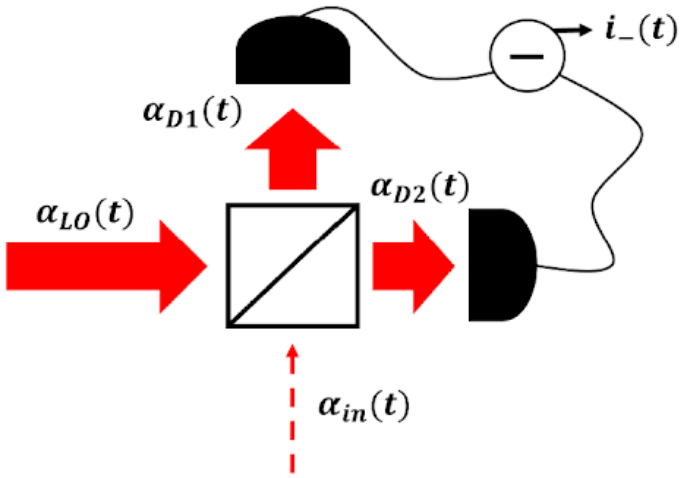

Figure 3.9: Homodyning detection using two photodiodes

The beam is sent to a 50:50 polarizing beam splitter and the two signals are detected by photodiodes D_1 and D_2 and then subtracted. The corresponding field amplitudes are

$$\alpha_{D1} = \frac{1}{\sqrt{2}}\alpha_{LO}(t) + \frac{1}{\sqrt{2}}\alpha_{sig}(t), \tag{3.3}$$

$$\alpha_{D2} = \frac{1}{\sqrt{2}}\alpha_{LO}(t) - \frac{1}{\sqrt{2}}\alpha_{sig}(t). \tag{3.4}$$

The photocurrent at each detector is proportional to the intensity given as

$$i_1 \propto |\alpha_{D1}|^2, \quad i_2 \propto |\alpha_{D2}|^2. \tag{3.5}$$

If we plug equation (3.3) and equation (3.4) into the expressions of i_1 and i_2 we get

$$i_1 \propto \left|\frac{1}{\sqrt{2}}(\alpha_{LO} + \alpha_{sig})\right|^2 = \frac{1}{2}\left(|\alpha_{LO}|^2 + |\alpha_{sig}|^2 + \alpha_{LO}^*\alpha_{sig} + \alpha_{LO}\alpha_{sig}^*\right). \tag{3.6}$$

$$i_2 \propto \left|\frac{1}{\sqrt{2}}(\alpha_{LO} - \alpha_{sig})\right|^2 = \frac{1}{2}\left(|\alpha_{LO}|^2 + |\alpha_{sig}|^2 - \alpha_{LO}^*\alpha_{sig} - \alpha_{LO}\alpha_{sig}^*\right). \tag{3.7}$$

Now to take the subtraction of the current, we see that

$$i = i_1 - i_2 \propto 2(\alpha_{LO}^*\alpha_{sig} + \alpha_{LO}\alpha_{sig}^*), \tag{3.8}$$

where

$$\alpha_{LO} = |\alpha_{LO}|e^{i\phi_{LO}}, \quad \alpha_{sig} = |\alpha_{sig}|e^{i\phi_{sig}}. \tag{3.9}$$

Therefore, we can see that

$$i \propto 2|\alpha_{LO}||\alpha_{sig}|\cos(\phi_{sig} - \phi_{LO}). \tag{3.10}$$

In the limit of a strong local oscillator ($|\alpha_{LO}| \gg |\alpha_{sig}|$), the current becomes

$$i \propto |\alpha_{LO}|\, X_\theta, \tag{3.11}$$

where X_θ is the signal field quadrature at phase angle $\theta = \phi_{LO}$. So Homodyning detection will result in the amplification of the weak vacuum squeezed field, or the noise quadrature projections.

The output of the photodiode subtraction from this detection scheem is shown in the right of figure 3.8. Notice that the amplitude interference fringes are visible, and there are portions of the signal that seem to "pause" the data collection. There is where the PZT physically resets, and must sweep back over the path it displaced the mirror. In post processing, we will segment the signal depicted in orange.

3.3.1 Spectrum Analyzer

The signal shown in the right of figure 3.8 is sent to a spectrum analyzer, which is a device that computes the magnitude of the signal relative to a frequency. Since the signal from the photodiode subtraction is only the noise component of the squeezed signal highlighted by the LO, the output on the spectrum analyzer is the noise power density. This is the intensity of the photodiode current given as

$$\langle i^2 \rangle \propto |\alpha_{LO}|^2 \langle \alpha_{sig}^2 \rangle, \tag{3.12}$$

which is equivalent to the quadrature variance representation. At some arbitrary phase, such measurement of $\langle i^2 \rangle$ could yield $\langle (q)^2 \rangle$, and at 90 degrees later $\langle (p)^2 \rangle$.

In simulation, the signal output of a true squeezed mode on the spectrum analyzer should look as pictured in figure 3.10,

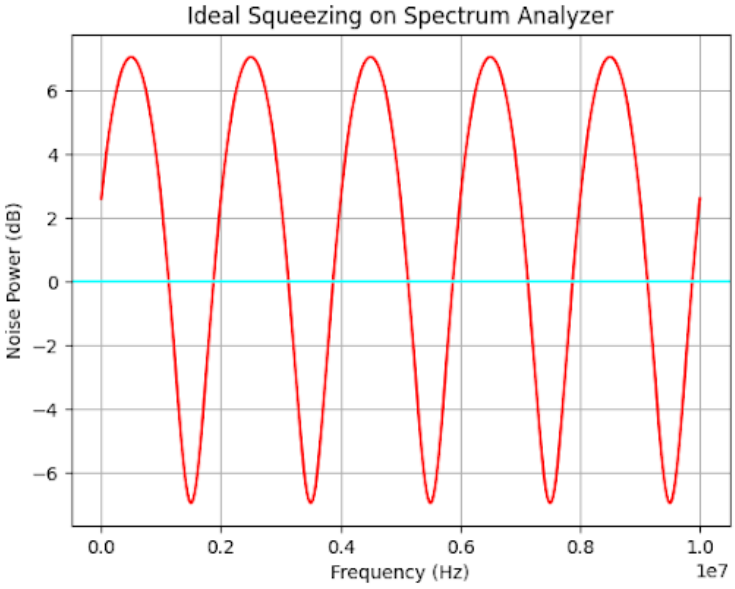

Figure 3.10: Ideal homodyning detection on spectrum analyzer for 1 true squeezed mode.

where the red signal is the photodiode subtraction, and the blue signal is the shot noise of the experimental system. Shot noise is the noise level where all classical

sources of noise are eliminated. Shot noise sits at the standard quantum limit of noise and classically no measurement can be more precise than shot noise. Notice that the red signal is equally biased above and below shot noise. This indicates true squeezing as the signal is just as squeezed as it is anti-squeezed. This must be true if the squeezing was applied to a coherent state as the area of phase space is always preserved. Additionally, the sine curve in figure 3.10 appears distorted since it is on a logarithmic scale. Every $3dB$ change in noise signal results in a 0.5 reduction of noise.

Experimentally, the output from the squeezer on to spectrum analyzer looks as shown in figure 3.11,

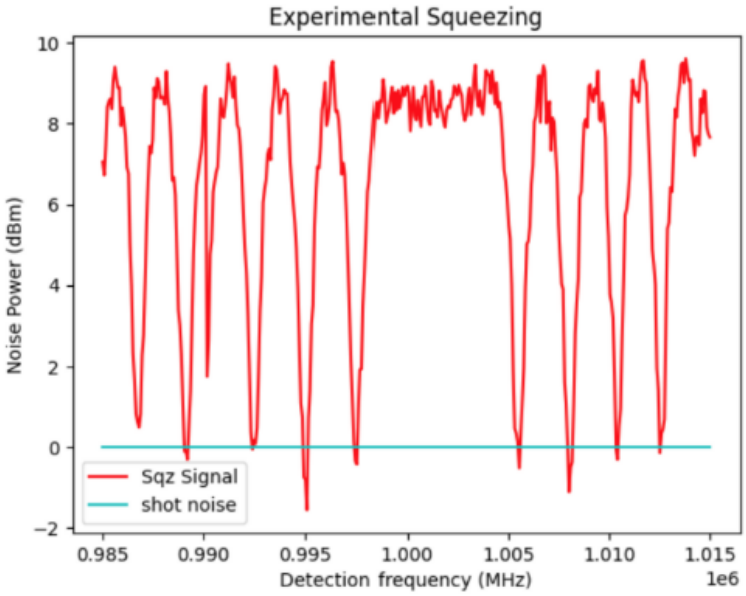

Figure 3.11: Photodiode subtraction of squeezed signal and shot noise measured on the spectrum analyzer. On average about $1db$ of squeezing is present on these particular photodiodes when measuring all modes in our experiment.

where shot noise is obtained by blocking the squeezing arm of the interferometer, eliminating any interference fringes. The PZT resets its sweep sequence for a finite amount of time as seen by the lack of peaks in the middle of the red signal, as

previously discussed and seen on the oscilloscope.

The periodic waveform of the red squeezed signal is created from the sweeping of the PZT, changing which portion of the noise ellipse projected onto the real axis. Notice the majority of the signal is greatly anti-squeezed. This looks different from the simulated model. It is evidence that there does not exist one pure single squeezed mode as if so, the degree of anti-squeezing and squeezing would be equivalent as shown in figure 3.10. This highlights as issue with out system as currently we do not have an experimental method to interrogate the individual modes within the entire multi-mode ensemble of states that are measured. The solution to this problem is introduced in the next section.

You may also notice that the degree of sub-shot noise signal values varies. This is because the overlap of the LO and signal beam changes as the PZT sweeps, and the degree of squeezing is very sensitive to this overlap. The alignment of the interferometer must be stable or squeezing detection will degrade. This amount of fluctuations in not optimal as each applied phase mask will already change the overlap. Changes in the signal contrast may now be from the phase masks and the PZT, making the data noisier. However this setup is sufficient for our purposes since we are not resolving many spatial modes. We may attempt to fix this issue in the future by changing the layout of the PZT and how it interacts with the beam path.

3.4 Shaping the Local Oscillator

To illuminate different sections of the squeezed signal and ultimately separate superimposed constituent modes, we must have control over the shape of the LO. Figure 3.11 is the output obtained when the entire LO interacts with the squeezed signal, but that signal contains the combination of many ideal true squeezed signals, as shown in figure 3.10, which we are interested in. It appears removing portions of the LO will

help deconstruct the superposition of outputs we measure. Modifying the phase of the LO will change the overlap between the LO and squeezed signal. This determines how much of a particular mode we measure of the signal beam. The spatial overlap of LO field u_{LO} and squeezed field u_{sig} can be expressed as

$$O = \int_A u_{LO}^* u_{sig}\, dA \tag{3.13}$$

over some area of detection A. When there is strong overlap between the LO and squeezed signal, meaning their beam shapes are aligned, the differential photocurrent measured by the balanced photodiode in equation (3.10) will have larger contrast. This means the amplitude of oscillation will be greater relative to a position of less overlap between the LO and signal.

In the path of the LO in figure 3, a device called a spatial light modulator is used to perform reshaping of the LO. The SLM is a liquid crystal optoelectronic device that allows the user control over the the refractive index of a particular "pixel" on the surface.

Nominally, an SLM is just a mirror but we will program its operation with a phase grating across the beam's profile. This causes the deflection of all diffraction orders away from the optical path, except for the 0th order we wish to operate in. Such deflection is required for effective use of the SLM as any desired programmed phase mask will be lost if all light is allowed to converge on the detector.

On top of the phase grating, we can program any desired phase mask to modify the LO. A logical way to break down spatial areas of the LO is imagining a superpixel grid that can be toggled ON and OFF. When in the ON state, we can measure the variance of the quadrature projection in that particular pixel. This method is well-suited to probing multimode squeezed states as the signal can be projected into a basis of spatial modes where we can measure individual and joint quadrature statistics [2].

Such phase masks will be pictured and discussed in the next chapter.

3.4.1 Local Oscillator Reference Beam

Since the LO propagates inside the interferometer, the intentional phase changes, done through pixel masks on the SLM, could be combined with additional phase variation from turbulence and vibration in the setup [2].This is undesirable but hard to eliminate. An easier solution is to correct for environmental phase fluctuations using a counter-propagating reference laser in the interferometer. Both experience the same optical elements but will posses orthogonal polarizations so that the reference beam is insensitive to the SLM's programmed phase masks. This is considered a phase-locking mechanism where the phase difference between the LO and the reference beam reveals the true phase of the SLM masks. The reference is detected and measured using a single photodiode detector.

Chapter 4

Data Collection

Returning to the goal of our measurement scheme, all elements of the squeezed mode ensemble covariance matrix Σ_d must be individually calculated. To fully interrogate each mode's quadrature noise, a series of phase masks can be applied on the SLM. The SLM is made of 512x512 physical pixels that are segmented into regions called superpixels. This experimentation works to resolve 4 spatial modes using 4 superpixels on the SLM. This can be visualized in figure 4.1. The region of interest (ROI) used for this experimentation is shown in red and reflects the size of the signal beam. Only where the LO and signal beam overlap will we observe squeezing. So we choose to work in this regime. The ROI was optimized for the greatest contrast of the squeezed signal, or spatial overlap.

4.1 Measurements

For every phase mask applied to the SLM, only 3 unique data collection take place: (1) The squeezed signal, (2) the reference signal, and (3) the shot noise or environment noise measurement. To resolve all elements of the covariance matrix, the squeezed signal is collected in 3 different ways to ensure accurate phase and amplitude measurements. To extract the quadratures from each mask, the PZT sweeps the LO's phase and we fit the resulting signal from the photodiode subtraction as

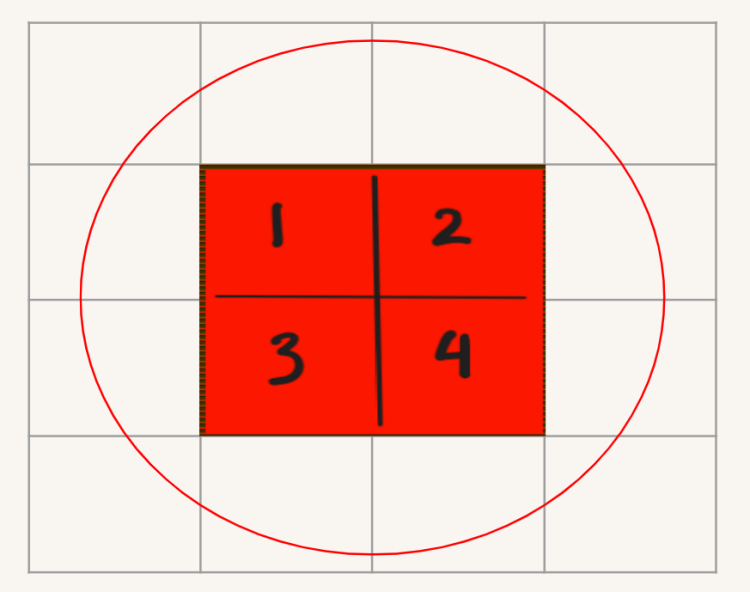

Figure 4.1: SLM mirror screen with LO beam cross section shown as a red circle. 4 super pixels are presented.

$$|i(\phi_{mask})|_{noise} = \frac{|(V_+ - V_-)|}{2} \cos(w_{PZT}t + \phi_{mask}) + b, \tag{4.1}$$

where $w_{PZT} = 2\pi \times 1$ Hz, V_+ and V_- are the maximum and minimum variances, making $|(V_+ - V_-)|$ the contrast of the signal, and b is the offset.

The 2 collections using the spectrum analyzer are the quadrature noise and shot noise traces taken in (dBm) from the photodiode subtraction as discussed in the last section. This output is curve fitted and shown in the top image of figure 4.3. 3 more collections are completed with an oscilloscope. The first 2 are the photodiode subtraction from the squeezing board and the LO reference from a single photodiode. Despite the quadrature variances being measured already on the spectrum analyzer, the squeezed signal's phase relative to the LO reference is needed as well to compare subsequent phase masks, warranting this additional measurement. An experimental example of this is shown in figure 4.2, where the data is fitted to obtain the relative phase shift $|\phi_{masks}|$ from equation (4.1) when the mask is applied.

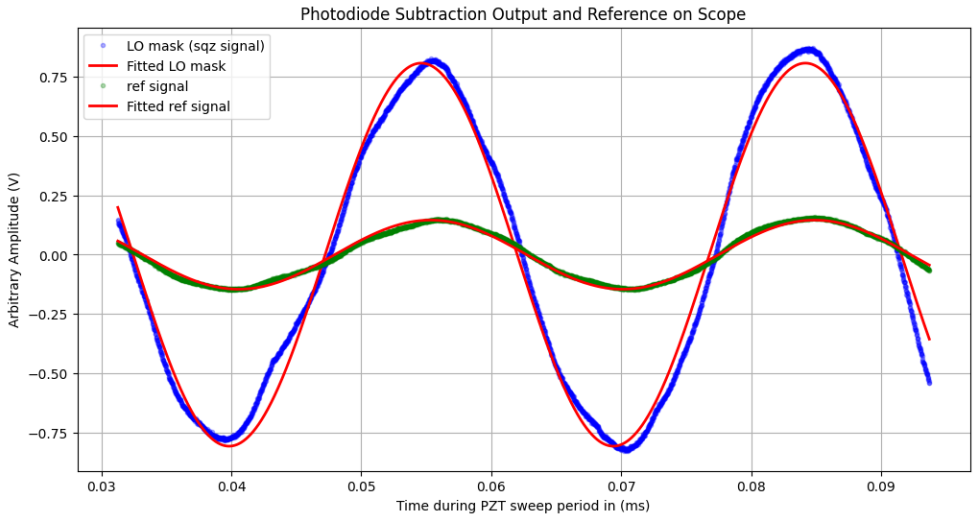

Figure 4.2: Experimental data of variance projections of the squeezed signal and the LO reference signal. The relative phase difference between these signals reflects different phase masks applied to the SLM. The reference signal will not be affected by the SLM.

The last measurement made with the scope is a projection of the quadrature variances measured by the spectrum analyzer made using a function called video out. This occurs because the scope and spectrum analyzer are not triggered to measure at the same point in time during the experiment. This means that a global phase shift, between the squeezed signal collected originally on the spectrum analyzer verses that collected on the scope, exists. The same phase value of the PZT must be translated between the scope and spectrum analyzer data to complete the covariance matrix calculations. An experimental example of the quadrature noise trace on the spectrum analyzer and its associated video output on the scope is shown in figure 4.3

Using curve fitting of equation (4.1), phase information from the reference signal can be translated into the time-domain of spectrum analyzer data. This is how the phase, or time position, of each quadrature q and p will be found.

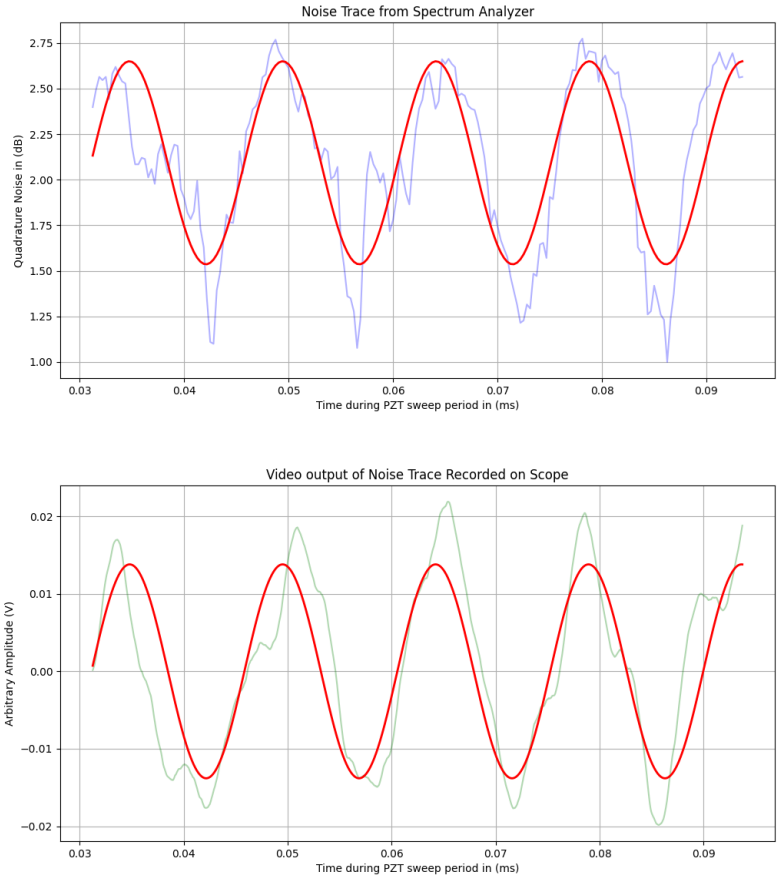

Figure 4.3: Experimental data of the quadrature noise variance recorded on the spectrum analyzer and the scope through the video out function.

4.2 Calculating the Covariance Matrix

The q_n and p_n values are of interest for every spatial mode. A series of phase masks are programmed to the SLM screen during the experiment to span all possible mode interactions in the covariance matrix given in equation (2.18).

There are 3 different orientations needed to obtain every individual covariance value in the entire matrix. The possible cases are shown in part b, c, and d of figure 4.4.

Beginning with case b, a pixel 1 toggled ON, from figure 4.4. This will allow us

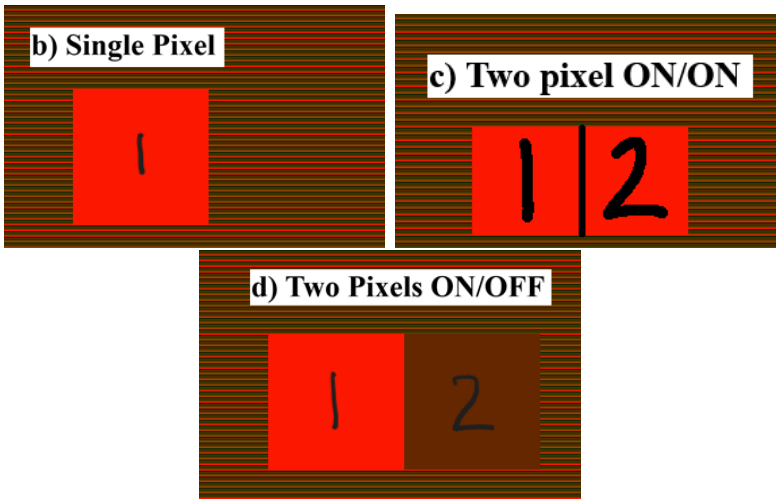

Figure 4.4: Phase masks sent to SLM
Part b is the case of single pixel measurements. Part c is the case of double pixel measurements both at the same phase. Part d is the case of double pixel measurements with a $\pi/2$ phase shift between them. "OFF" denotes this $\pi/2$ phase shift relative to "ON." Note that the stripped pattern in the background is the blaze grating used to isolate the 0^{th} order of the light beam.

to measure

$$\langle q_1^2 \rangle \tag{4.2}$$

and at a $\pi/2$ phase shift relative to the reference signal,

$$\langle p_1^2 \rangle \tag{4.3}$$

and at a $\pi/4$ phase shift relative to the reference signal,

$$\frac{1}{2}\langle (q_1 + p_1)^2 \rangle = \frac{1}{2}\left(\langle q_1^2 \rangle + \langle p_1^2 \rangle + 2\langle q_1 p_1 \rangle\right), \tag{4.4}$$

which can be simplified to

$$\langle q_1 p_1 \rangle = \frac{1}{2}\left(\langle (q_1 + p_1)^2 \rangle - \langle q_1^2 \rangle - \langle p_1^2 \rangle\right) = c(q_1, p_1). \tag{4.5}$$

This measurement is shown in part a) of figure 4.5. Similarly, with case c, pixel 2 and 3 toggled ON, from figure 4.4. This will allow us to measure

$$\frac{1}{2}\langle(q_2+q_3)^2\rangle = \frac{1}{2}\left(\langle q_2^2\rangle + \langle q_3^2\rangle + 2\langle q_2 q_3\rangle\right) \tag{4.6}$$

and at a $\pi/2$ phase shift relative to the reference signal,

$$\frac{1}{2}\langle(p_2+p_3)^2\rangle = \frac{1}{2}\left(\langle p_2^2\rangle + \langle p_3^2\rangle + 2\langle p_2 p_3\rangle\right), \tag{4.7}$$

which can be rearranged to

$$\langle q_2 q_3\rangle = \frac{1}{2}\left(\langle(q_2+q_3)^2\rangle - \langle q_2^2\rangle - \langle q_3^2\rangle\right) = c(q_2, q_3) \tag{4.8}$$

and

$$\langle p_2 p_3\rangle = \frac{1}{2}\left(\langle(p_2+p_3)^2\rangle - \langle p_2^2\rangle - \langle p_3^2\rangle\right) = c(p_2, p_3). \tag{4.9}$$

This measurement is shown in part b) of figure 4.5. Finially this process repeats with case d, pixel 1 toggled ON and pixel 2 toggled OFF, from figure 4.4. This will allow us to measure

$$\frac{1}{2}\langle(p_2+q_1)^2\rangle = \frac{1}{2}\left(\langle p_2^2\rangle + \langle q_1^2\rangle + 2\langle q_1 p_2\rangle\right) \tag{4.10}$$

and at a $\pi/2$ phase shift relative to the reference signal,

$$\frac{1}{2}\langle(q_2+p_1)^2\rangle = \frac{1}{2}\left(\langle q_2^2\rangle + \langle p_1^2\rangle + 2\langle q_2 p_1\rangle\right), \tag{4.11}$$

which can be rearranged to

$$\langle q_1 p_2\rangle = \frac{1}{2}\left(\langle(p_2+q_1)^2\rangle - \langle p_2^2\rangle - \langle q_1^2\rangle\right) = c(q_1, p_2) \tag{4.12}$$

and

$$\langle q_2 p_1\rangle = \frac{1}{2}\left(\langle(q_2+p_1)^2\rangle - \langle q_2^2\rangle - \langle p_1^2\rangle\right) = c(q_2, p_1). \tag{4.13}$$

This measurement is shown in part c) of figure 4.5.

The data in the figure gives us all the information needed to calculate every element in the covariance matrix Σ_d. Notice how the entire covariance matrix for 1 mode is filled up by these measurements. 3 more iterations of these measurements on different pixels will complete the measurement.

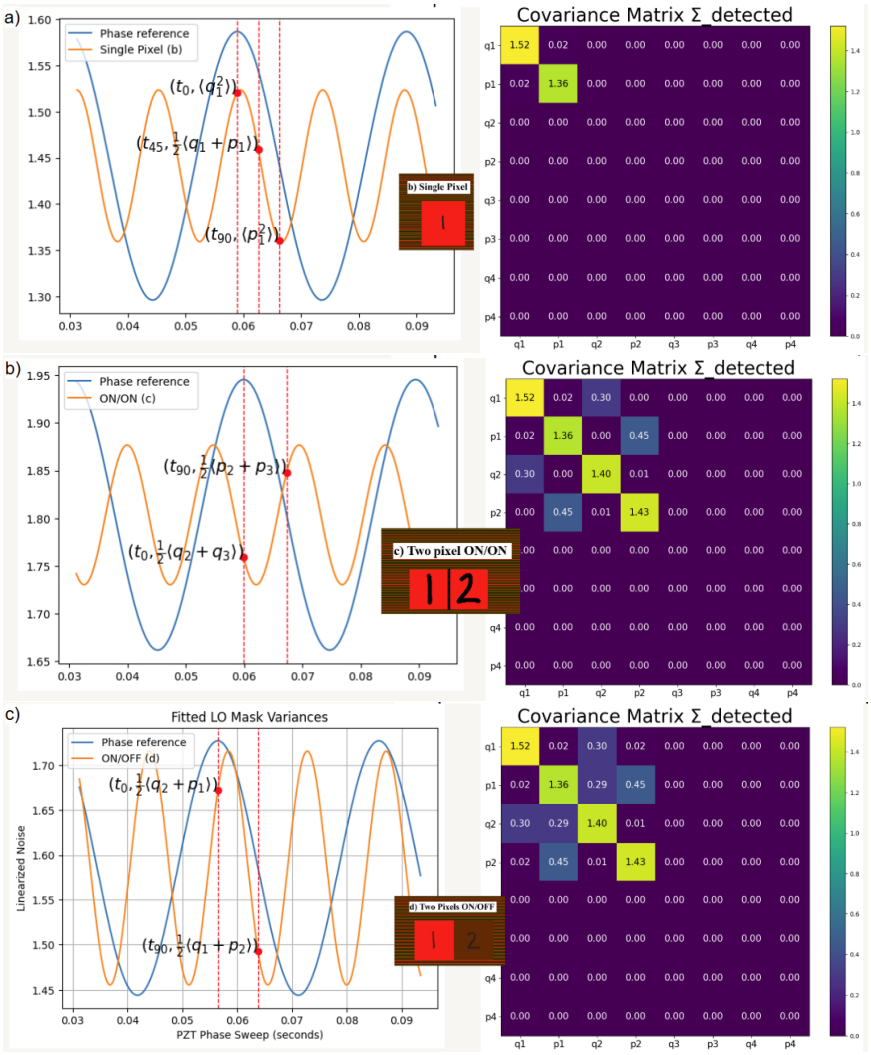

Figure 4.5: All critical measurement points from fitted collected data. Each curve corresponds to a measurement from figure 4.4.

Chapter 5

Postprocessing

To obtain Σ_o from equation (2.24), we need to find the reversible linear transforms C. Since Σ_d is a measurement that we experimentally obtained and by applying decompositions to this output, we can figure out what linear transformations occured [2]. The backwards propagation, or reconstruction, as shown in figure 2.8 is completed by a Williamson and then a Bloch-Messiah Decomposition. This process is modified from the open source quantum photonic algorithm Strawberry Fields [10]. The covariance matrix Σ_d is rearranged for the decompositions in the format $\vec{X}_n = (q_1, q_2, \ldots, q_n, p_1, p_2, \ldots, p_n)$, referred to as block form.

5.1 Shake Out of Covariance Matrix

As mentioned in section 2.6 and equation (2.12), the covariance matrix must be physical to undergo decompositions. Since the quadrature amplitude and phase data can be noisy from imperfect optical elements (beam splitters and waveplates) and inconsistent overlap between PZT sweeps, the raw output covariance matrix Σ_O is likely non-physical. We restore the physicality of parameters by modifying the raw output using a shake-out algorithm devised by Charris Gabaldon [2]. Using an optimizer, we create a 3 parameter cost function. The first parameter ensures the changes to each matrix element are at a minimal distance from its original value. This param-

eter is essential as any unnecessary alteration to the measured data could corrupt the underlying physical phenomena we are interested in [2]. The second parameter certifies that the average photon count is physical. The third parameter upholds real and positive eigenvalues. Below in figure 5.1 is before and after the application of the shake-out algorithm to experimental data of 4 spatial modes.

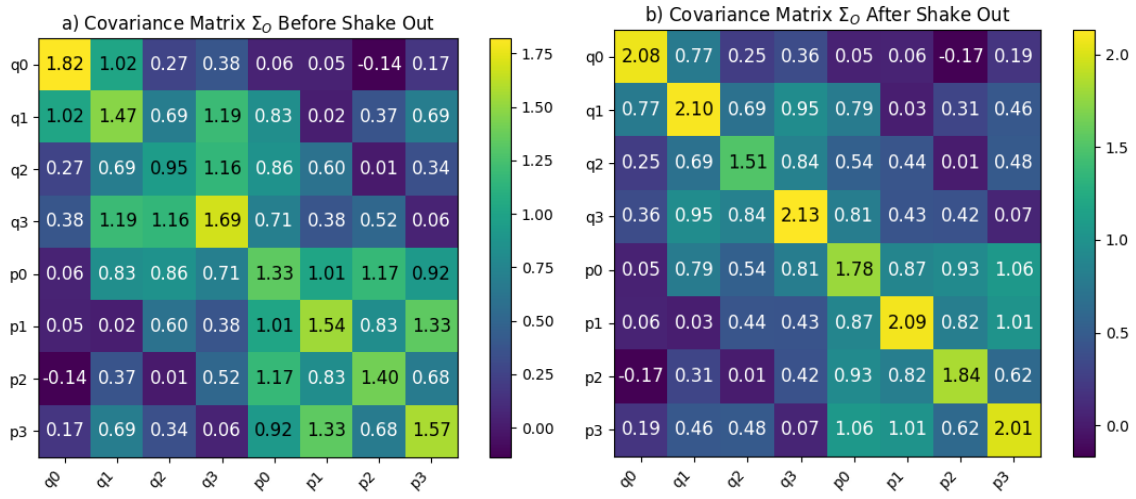

Figure 5.1: Experimental covariance matricies before (left) and after (right) the shake-out algorithm.

Notice that the color structures are somewhat similar between the two matricies but the values are slightly different.

5.2 Williamson Decomposition

The Williamson decomposition is described as

$$\Sigma_d = SDS^T, \tag{5.1}$$

where S is a transformation acting on the diagonal matrix D, describing the input thermal modes present. Each diagonal element in D can be expressed as $D_k = n_k + 1$, where n is the photon number of the k^{th} mode [2]. Eigenvalues of 1 in matrix D

represents a vacuum state. Ideally we would observe all vacuum modes, but there is thermal contamination in practice as discussed in section 2.4.1.

5.3 Bloch-Messiah Decomposition

The Bloch-Messiah Decomposition decomposes the matrix S from the Williamson decomposition and is described as

$$S = U\Sigma_o O_2, \tag{5.2}$$

where U and O_2 are matrices that hold linear transformation information [2]. In block form, the desired covariance matrix Σ_d holds the antisqueezing and squeezing parameter information as Σ_o =diag$(e^{r_1}, \ldots, e^{r_n}, e^{-r_1}, \ldots, e^{-r_n},)$. In a perfect vacuum squeezed mode, the anti-squeezing is equal and opposite of the squeezing parameter.

5.4 Extracting Spatial Modes

The matrix U contains the relevant amplitude and phase of each resolved spatial mode. To calculate this, we break up the U into four quadrants. The top left indicates the real portion of the modes A, and the top right indicates the complex part of the modes B. We can unwrap this information as $u = A + iB$, where each column of matrix U constitutes one reconstructed mode [2]. This can be visualized with 4 spatial modes, in the top figure 5.2. The red markup depict the square-root of the amplitude values and phase values of the first spatial mode. The reconstruction matrix U is shown in the bottom of figure 5.2 for each superpixel programmed to the SLM. From this, the quantum spatial modes can be fully described.

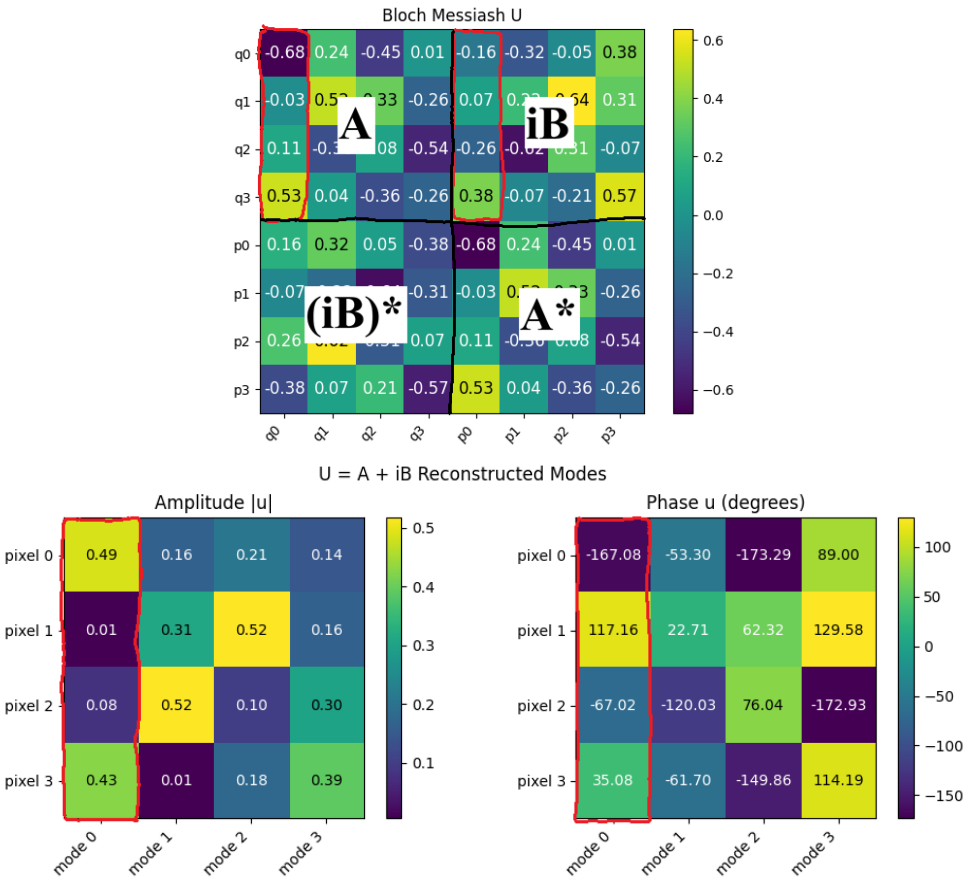

Figure 5.2: Experimental data of matrix O_1 (top) and its unwrapped reconstruction (bottom). The redmarks depict how each column maps to a spatial mode is reconstructed from this matrix.

Chapter 6

Discussion

In this section we will review the experimental results of this project and what implications they have.

6.1 Simulated Results

From both of the decompositions, we can extract the thermal field, squeezed field, and anti-squeezed field of our data. An example of this is shown in figure 6.1. The thermal field reports the amount of total noise in each mode. Since a vacuum state was the input of this experiment, we would hope to measure vacuum squeezed modes as a result, which are depicted in part a) of the figure. Shot noise, or the standard quantum limit of noise is normalized to a value of 1 in this experiment, so all of these modes exhibit this. However, this does not occur in practice, as spontaneous emission cannot be eliminated in the atomic vapor cell. Therefore, it is likely that some modes will contain thermal contamination and exhibit total noise above the shot noise level. This will result in values greater than 1 in this field.

In the application of quantum information, this is acceptable as the relevant information will be stored in the squeezing parameter. In a quantum metrology application, any thermal mode will degrade the possibly squeezing effect relative to the shot noise of the system. The presence of vacuum modes in our data will indicate

successful experimentation, as none would question the connection to our input state.

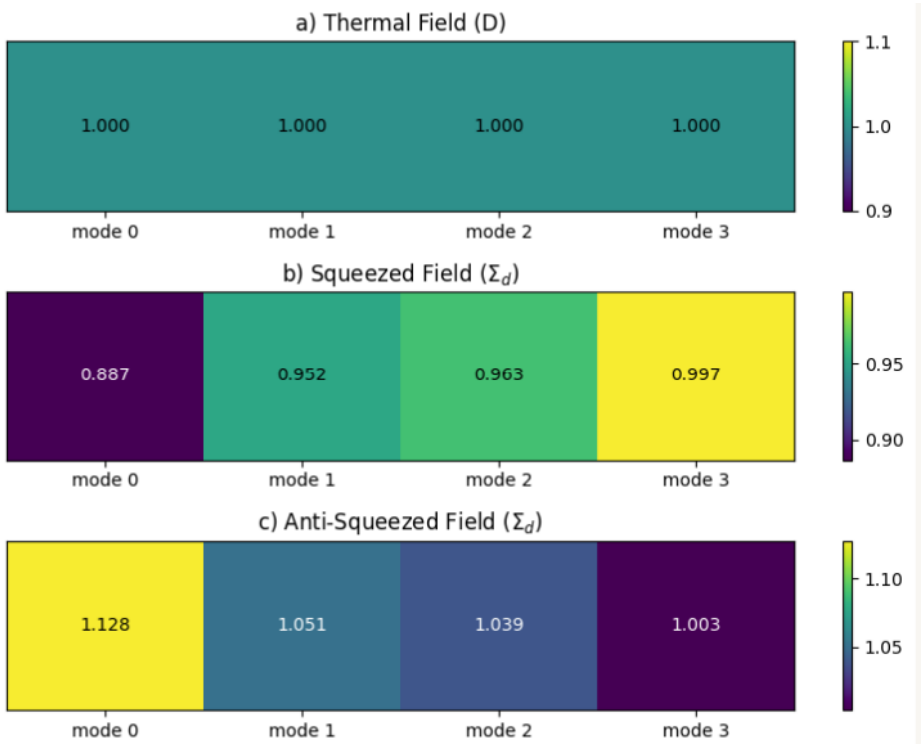

Figure 6.1: Simulation data: a) Thermal field b) squeezed field c) anti-squeezed field.

The squeezed field and anti-squeezed field are the from

$$\Sigma_o = diag(e^{r_1}, \ldots, e^{r_n}, e^{-r_1}, \ldots, e^{-r_n}). \tag{6.1}$$

Notice that these values are equally spaced from the shot noise value of 1, and are effectively multiplied to the thermal state. For example, mode 0 has $e^{-r_0} = 0.887$, yielding a value of $r = 0.120$ for the squeezing parameter. The noise power will scale as $e^{-2r} = 0.787$ which is equivalent to $10log_{10}(0.787) = -1.04$ dB of squeezing. There is about 1 dB of anti-squeezing as well.

About $1dB$ of input squeezing was measured from all the modes in figure 3.11, an indication of success would be to resolve a squeezed mode of greater value. This will align with out prediction that the combination of many true modes creates less squeezing.

6.2 Experimental Results

Four spatial modes have been measured and reconstructed in this experiment. 10 trials have been observed and the averaged results are given in figure 6.2. We can see

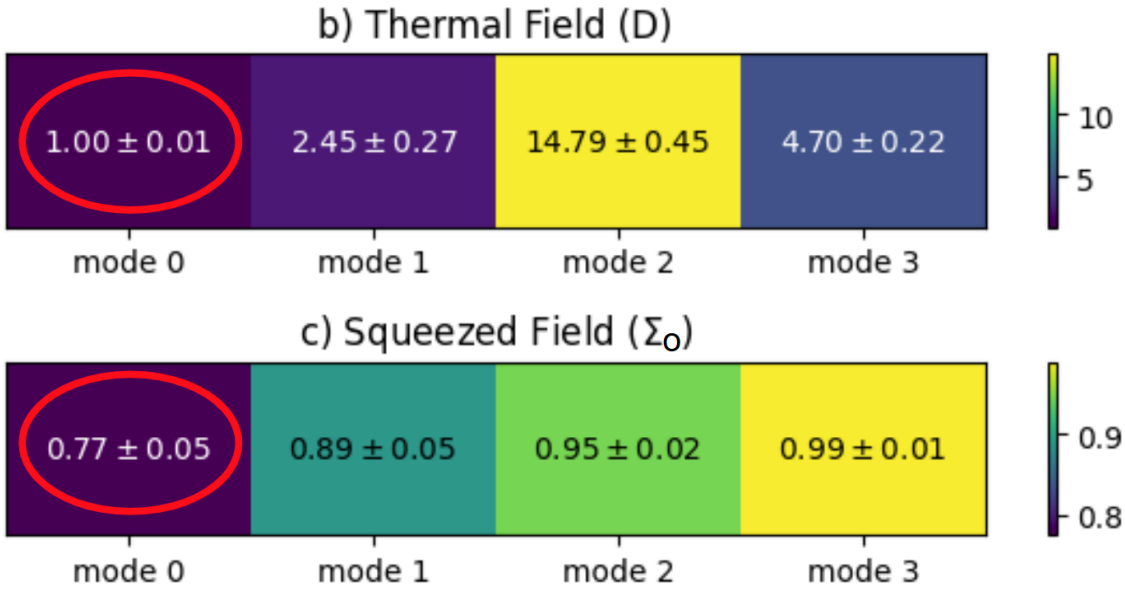

Figure 6.2: Experimental results: b) Thermal modes from Williamson decomposition, c) Squeezed modes from Σ_d

from the data that there is consistently 1 strong thermal mode and 1 truely squeezed vacuum mode circled in red. Using basic calculations, mode 0 is found to be squeezed -2.27 dB, which is larger than the total squeezing measured from all modes. This verifies we were measuring what we were predicting is occuring in the multi-mode squeezer.

The average amplitude and phase of each mode was calculated using the method previously discussed and is shown in figure 6.3. It's useful to note that modes with total noise above the standard quantum limit will have greater amplitude as there are more photons present. However, this is not present in this image as all results are normalized. Since there are so few superpixels, it is hard to resolve significant

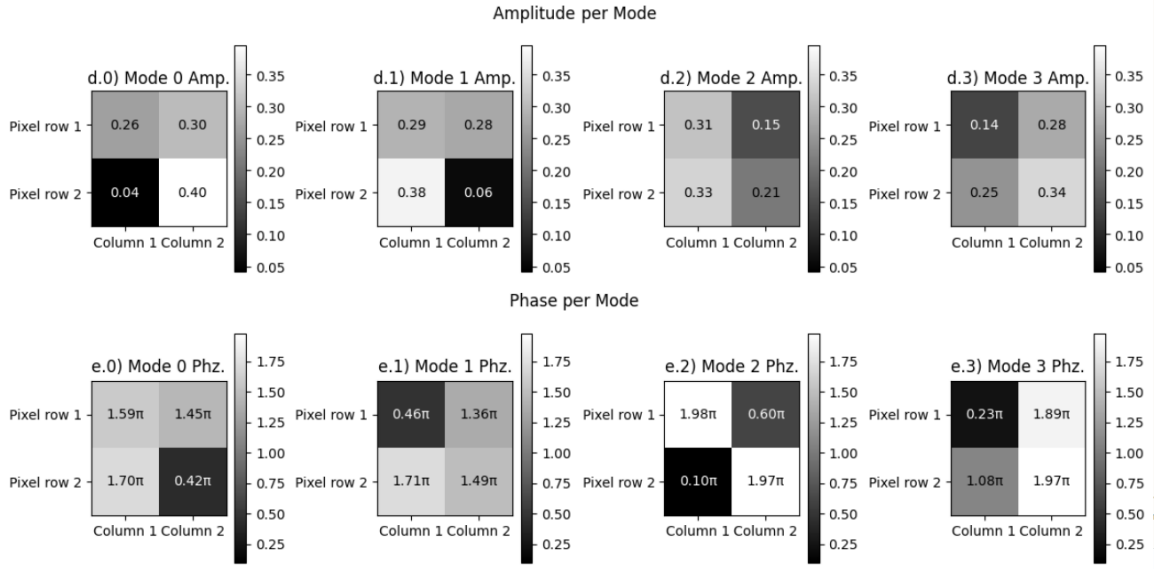

Figure 6.3: Quantum Spatial Modes: d) normalized amplitudes of each mode, e) phase component of each pixel of each mode

structures in the squeezed quantum spatial modes. However, they all seem biased to 1 particular corner when looking qualitatively. The goal of this work was to image quantum structures that we have never seen before, and in this figure, we accomplish just this.

Chapter 7

Conclusion and Outlook

This thesis has developed a novel method to measure and reconstruct squeezed quantum spatial modes of light. Using a multi-mode squeezer, the squeezed signal was measured using an interferometer and balanced homodyne detection. Key values in the covariance matrix describing the quantum structure of the spatial modes were extracted from the experimental measurement using phase and amplitude tracking information. Then a novel reconstruction of the original modes was performed using decompositions to yield the amplitude and phase of every superpixel per mode. 4 modes were resolved in this experimentation, 1 of which were truly squeezed. These results indicate successful reconstruction of 4 spatial modes as a squeezed mode was observed with larger squeezing than the entire ensemble. This is the first demonstration of such reconstruction without prior knowledge of mode shapes.

Future iterations of this experiment will strive to resolve more pixels so features of the spatial amplitude and phase distribution can be identified in the quantum modes. As shown in part a) of figure 7.1, a 3x3 grid of superpixels would be a natural next step. Increasing superpixels will be achieved by using more power to ensure the data signal is not corrupted by photodiode dark noise. Parameters that govern optimal squeezing in our vapor cell could be optimized as well to possibly yield more squeezing and less thermal modes. This could make our experimental method more applicable

to metrology goals and also help the effort to resolve more superpixels or quantum spatial modes for information purposes.

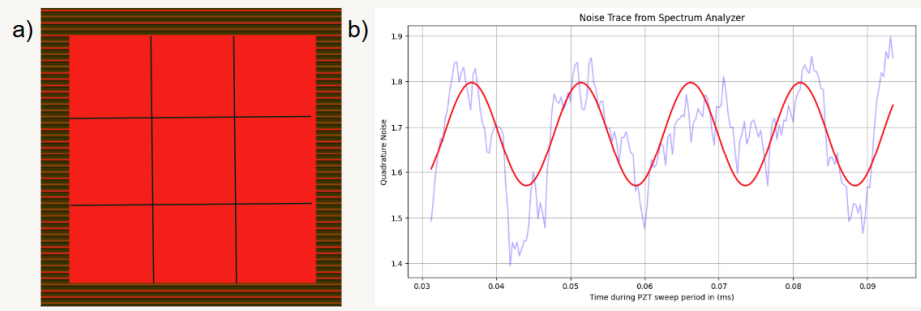

Figure 7.1: Areas of future improvement: a) adding more pixels b) decreasing experimental noise when measuring quadratures.

In general, improving the sensitivity of phase reconstruction is an important challenge to overcome in this work, as quadratures measurements are susceptible to noise [2]. This could include better experimental control over the PZT, and other noise mitigation methods. As shown in part b) of figure 7.1, the sinusoidal fit of the noisy spectrum analyzer data could be artificially inserting squeezing or thermal features in our data. Obtaining data with high signal to noise ratio is imperative to resolving more quantum squeezed spatial modes.

Our experimentation has shown that squeezed states, which are an important tool in quantum metrology, can be identified even when spatially overlapped. This demonstration could serve as a readout method for quantum information science applications, like in high-dimensional quantum networking. However, methods for encoding information within these quantum spatial modes would need to be created for this to be useful. The first step in this process is confirming their detection and measurement possibilities, which this thesis has contributed to.

References

[1] Philip R. Bevington and D. Keith Robinson. *Data Reduction and Error Analysis for the Physical Sciences*. 3rd. McGraw-Hill, 2003.

[2] Charris Gabaldon. "Squeezed Quantum Spatial Mode Reconstruction". PhD thesis. College of William & Mary, 2025.

[3] Li Ge and Demetrios N. Christodoulides. "Quantized Nonlinear Gaussian-Beam Dynamics Tailoring Multimode Squeezed-Light Generation". In: *Phys. Rev. Lett.* 131 (11 July 2023), p. 113601. DOI: 10.1103/PhysRevLett.131.113601. URL: https://link.aps.org/doi/10.1103/PhysRevLett.131.113601.

[4] Savannah Cuozzon. "Quantum Sensing for Low-Light Imaging". PhD thesis. College of William & Mary, 2022.

[5] Wikipedia contributors. *Squeezed states of light*. https://en.wikipedia.org/wiki/Squeezed_states_of_light. Accessed: 2026-05-07. n.d.

[6] "Quantum Models of Light". In: *A Guide to Experiments in Quantum Optics*. John Wiley & Sons, Ltd, 2004. Chap. 4, pp. 60–98. ISBN: 9783527619238. DOI: https://doi.org/10.1002/9783527619238.ch4. eprint: https://onlinelibrary.wiley.com/doi/pdf/10.1002/9783527619238.ch4. URL: https://onlinelibrary.wiley.com/doi/abs/10.1002/9783527619238.ch4.

[7] Eugeniy E. Mikhailov and Irina Novikova. "Low-frequency vacuum squeezing via polarization self-rotation in Rb vapor". In: *Optics Letters* 33.11 (2008), pp. 1213–1215. DOI: 10.1364/OL.33.001213.

[8] Bijan Bagchi, Rupamanjari Ghosh, and Avinash Khare. "A pedestrian introduction to coherent and squeezed states". In: *International Journal of Modern Physics A* 35.19 (July 2020), p. 2030011. ISSN: 1793-656X. DOI: 10.1142/s0217751x20300112. URL: http://dx.doi.org/10.1142/S0217751X20300112.

[9] Savannah Cuozzo et al. "Low-Light Shadow Imaging Using Quadrature-Noise Detection with a Camera". In: *Advanced Quantum Technologies* 5.5 (2022), p. 2100147. DOI: 10.1002/qute.202100147.

[10] Nathan Killoran et al. “Strawberry Fields: A Software Platform for Photonic Quantum Computing”. In: *Quantum* 3 (Mar. 2019), p. 129. ISSN: 2521-327X. DOI: 10.22331/q-2019-03-11-129. URL: https://doi.org/10.22331/q-2019-03-11-129.